# DESIGN OF

# ULTRA-STRETCHABLE NANOMESH

# STRUCTURES

By

OISHWARYA BHOWMIK
Bachelor of Science in Mechanical Engineering
Bangladesh University of Engineering and Technology
Dhaka, Bangladesh
2018

Submitted to the Faculty of the
Graduate College of the
Oklahoma State University
in partial fulfillment of
the requirements for
the Degree of
Master of Science
JULY, 2022

DESIGN OF

ULTRA-STRETCHABLE NANOMESH

STRUCTURES

Dissertation Approved:

Dr. Shuodao Wang

Dissertation Advisor

Dr. Kaan Kalkan

Dr. He Bai

## ACKNOWLEDGMENTS

I would want to extend my gratitude to my adviser, Dr. Wang, for his ongoing advice and assistance. Without his assistance and supervision, it would be challenging to complete my thesis. He allowed me quite enough freedom to feel at ease with my work and let me go exploring on my own to hone my talents. I also want to express my gratitude to Dr. He Bai and Dr. Kaan Kalkan, who served as my committee member, for their time and insight on this thesis.

I appreciate my friends and colleagues for their support both in and out of the classroom, as well as for the useful and informative conversations we had regarding my research and academics.

Finally, I want to express my sincere gratitude to my beloved parents, Himadry Shekhar Bhowmik and Lipika Mazumder, as well as my brothers Aitijya Bhowmic and Aditya Bhowmic, for their unconditional support and affection. I am fortunate enough to have them supporting me in all areas of my life, and their continuous motivation to reach my goals despite all obstacles.

Acknowledgments reflect the views of the author and are not endorsed by committee members or Oklahoma State University.

Name: OISHWARYA BHOWMIK

Date of Degree: JULY, 2022

Title of Study: DESIGN OF ULTRA-STRETCHABLE NANOMESH STRUCTURES

Major Field: MECHANICAL AND AEROSPACE ENGINEERING

Abstract:

Wide-ranging applications of integrated stretchable electronics, including sensors, actuators, energy harvesting, etc., are made possible by expeditious advancements in design and materials. Nanomesh structures brought a significant development in this field showing excellent transparency, lower stiffness, and high stretchability. This thesis studies the mechanical properties of hexagonal nanomesh structures made of arc-shaped serpentine traces. Theoretical and finite element models are developed to investigate the displacement, maximum strain, axial stiffness, stretching rigidity, effective modulus, and stretchability of the hexagonal nanomesh structures for different thicknesses and arc-angles of the traces. The findings of the analytical process appear to be matched very well with the finite element analysis results. As a result, these verified theoretical formulations can be used to have practical instructions for constructing the nanomesh structures to achieve very higher stretchability and mechanical qualities, which are highly desirable properties in manufacturing wearable electronics and bio-mimetic structures.

TABLE OF CONTENTS

Chapter Page

**I. Introduction and Background Information . . . . . 1**

1.1 Introduction . . . . . 1

1.1.1 Motivation . . . . . 1

1.1.2 Objectives . . . . . 6

1.2 Background Information . . . . . 6

1.2.1 Elastic Modulus . . . . . 6

1.2.2 Stiffness of Material . . . . . 6

1.2.3 Stretching Rigidity . . . . . 7

1.2.4 Nanomesh Structures . . . . . 7

1.2.5 Finite Element Analysis . . . . . 8

**II. Analytical Approach to Calculate the Mechanical Properties of the Hexagonal Nanomesh Structure . . . . . 9**

2.1 Unit Cell . . . . . 9

2.2 Stretching of Hexagonal Nanomeshes in the x-direction . . . . . 10

2.2.1 Displacement of the Inclined Trace . . . . . 10

2.2.2 Displacement of the Horizontal Trace . . . . . 14

2.2.3 Displacement of the Unit Cell . . . . . 15

2.2.4 Effective Modulus and Stretchability of the Nanomesh . . . . . 15

2.3 Stretching of Hexagonal Nanomeshes in the y-direction . . . . . 17

2.3.1 Displacement of the Unit Cell . . . . . 18

2.3.2 Effective Modulus and Stretchability of the Nanomesh . . . . . 18

Chapter Page

**III. Finite Element Model of the Hexagonal Nanomesh Structure . . . . 21**

3.1 Simulation of the Structure . . . . . 21

3.1.1 Create Part . . . . . 21

3.1.2 Material and the Properties . . . . . 21

3.1.3 Boundary Conditions . . . . . 22

3.1.4 Mesh Generation . . . . . 23

3.1.5 Effective Modulus . . . . . 23

**IV. Effective Moduli and Stretchability of the Nanomesh Structure for Different Geometric Parameters . . . . . 26**

4.1 Effective Moduli due to Stretching in the x-direction . . . . . 26

4.2 Effective Moduli due to Stretching in the y-direction . . . . . 27

4.3 Maximum Strain and Stretchability along the x-Direction . . . . . 27

4.4 Maximum Strain and Stretchability along the y-Direction . . . . . 28

4.5 Results and Discussion . . . . . 29

**V. Conclusion and Future Work . . . . . 34**

5.1 Conclusion . . . . . 34

5.2 Future Work . . . . . 34

**REFERENCES . . . . . 35**

LIST OF FIGURES


| Figure | | Page |
|---|---|---|
| 1 | Uses of Nanomesh: (a) A breathable electronic skin [27] and (b) Conductor created by gold nanomesh [27], (c) Electronic eyeball camera [31], (d) Stretchable LED display instruments that use mesh patterns with microscale inorganic Light-emitting diodes [31] and (e) Stretchable silicon circuit with a mesh pattern (left), wrapped onto a structure of a fingertip, presented at low (left), medium (center) and high (right) magnification [31]. . . . . | 2 |
| 2 | Self-similar Serpentine Inter-connectors: (a) Non-coplanar serpentine wires on fully inflated balloon of cardiac machine [39] and (b) Deformation of self-similar serpentine wires for various levels of applied tensile strain [43] | 3 |
| 3 | Hexagonal nanomesh structures of Graphene made of carbon atoms [3] . | 8 |
| 4 | (a) Arc-shaped serpentine hexagonal nanomesh and (b) Unit cell . . . . | 9 |
| 5 | Stretching of the mechanical model of arc-shaped serpentine hexagonal nanomesh in x-direction: (a) Undeformed (dashed lines) and deformed (solid lines) structure of the unit cell,(b) force analysis of the inclined trace and (b) force analysis of the horizontal trace . . . . . | 10 |
| 6 | (a) Force analysis of inclined trace and (b) virtual cut on the trace . . . | 11 |
| 7 | Unit cell dimensions. . . . . | 15 |
| 8 | Bending moments on a single trace. . . . . | 16 |
| 9 | Stretching of the mechanical model of arc-shaped serpentine hexagonal nanomesh in y-direction: (a) Undeformed (dashed lines) and deformed (solid lines) structure of the unit cell,(b) Internal force analysis . . . . . | 17 |
| 10 | Unit cell dimensions. . . . . | 19 |
| 11 | Section Sketch of a 16 by 16 Hexagonal Nanomesh Structure . . . . . | 22 |
| 12 | Boundary Conditions on a Part of the Large Hexagonal Nanomesh Structure: Blue nodes: U1=UR3=0, Red nodes: U1=given value of $\Delta_x$, UR3=0, Purple Nodes: U2=UR3=0, Green Nodes: UR3=0, U2 of the green nodes= U2 of node 1, where U1= displacement along the x-axis, U2= displacement along the y-axis, UR3= rotational displacement along the z-axis. . . . . | 23 |
| 13 | Boundary Conditions on a Part of the Large Hexagonal Nanomesh Structure: Blue nodes: U2=UR3=0, Red nodes: U2=given value of $\Delta_y$, UR3=0, Purple Nodes: UR3=0, U1 of the Purple Nodes = U1 of Node2 Green Nodes: U1=UR3=0, U1= displacement along the x-axis, U2= displacement along the y-axis, UR3= rotational displacement along the z-axis. . | 24 |

Figure Page

14 Mesh Generation . . . . . 24
15 Reaction forces generated due to stretching in the x-direction . . . . . 25
16 Effective moduli($E_{x-eff}$) of the nanomeshes versus arc angle ($2\theta_0$) . . . . 26
17 Normalized effective modulus ($\frac{E_{x-eff}}{E}$) versus arc angle ($2\theta_0$) . . . . . 27
18 Effective moduli($E_{y-eff}$) of the nanomeshes versus arc angle ($2\theta_0$) . . . . 28
19 Normalized effective modulus ($\frac{E_{y-eff}}{E}$) versus arc angle ($2\theta_0$) . . . . . 28
20 Maximum Strain of the nanomeshes from Finite Element Analysis for the traces of arc-angle 112.5 °and thickness of (a) 18nm, (b) 9nm and (c) 6nnm. Given that the deformation is periodic, only representative nanomeshes are shown. . . . . 29
21 Maximum Strain of the nanomeshes from Finite Element Analysis for the traces of arc-angle 135 °and thickness of (a) 18nm, (b) 9nm and (c) 6nnm. Given that the deformation is periodic, only representative nanomeshes are shown. . . . . 30
22 Maximum Strain of the nanomeshes versus arc angle ($2\theta_0$) . . . . . 31
23 Normalized Stretchability of the nanomeshes versus arc angle ($2\theta_0$) . . . 31
24 Maximum Strain of the nanomeshes versus arc angle ($2\theta_0$) . . . . . 32
25 Normalized Stretchability of the nanomeshes versus arc angle ($2\theta_0$) . . . 32

# CHAPTER I

## Introduction and Background Information

### 1.1 Introduction

#### 1.1.1 Motivation

Stretchable electronics have drawn much attention over the past years because they offer excellent performance and extraordinary deform-ability simultaneously that make them stand out from conventional electronics [13] [17] [18] [21] [22] [32] [33]. Nanomesh structures brought a significant development in the field of stretchable electronic systems (Figure 1). To list a few among such developments, the technology of bilayer nanomesh microelectrodes is anticipated to enable next-generation transparent large-scale bioelectronics with a wide range of biological applications [29], the translucent and highly flexible Au nanomesh electrodes hold promise for use in muscle-like transducers and foldable photoelectronics [14]; with applications ranging from on-skin electronics to implanted biomedical devices, a wafer-scale nondestructive transfer approach using an ultrathin polyimide layer offers a realistic route towards producing large-scale stretchy electronics based on nanomesh [34], the technology of metal nanomesh films made with the AAO template offer a fresh idea for creating transparent metal electrodes that are also stretchable for use in future electrical devices [15], the performance of electrochromic polymers in applications such as smart windows or displays can be improved and controlled using nanostructured system technology [36]. For microelectronic applications, the good control of the sheet resistance and transmittance given by the metal mesh electrodes is very advantageous. As a result, numerous studies have been carried out over the last ten years in an effort to create high-performance metal mesh. Combining colloidal deposition with silver enhancement processes results in a novel method for producing durable silver mesh without the use of risky organic solvents [19]. For continuous motion activity monitoring that eliminates mechanical restrictions on natural skin motions, a technology of an ultra-thin and robust nanomesh strain gauge is created. Ultra-conformable strain gauges have found extensive use in treatments, interactive robotics, human motion detection, and personal health monitoring. They can be directly placed to human skin for continuous motion activity monitoring. This is another striking example of applications of nanomesh technology [42].

A popular method for creating stretchy bio-integrated electronics is to pattern rigid materials into self-similar serpentine-shaped ribbons. (Figure 2).

It has been found that serpentine strands show much higher intrinsic fracture of strain of 40% [45] and research works have been being done to improve the performances of the electronics using serpentine structures and studying their mechanical characteristics. Like, the stretchability of two serpentine-based and one spiral-based copper interconnects are com-

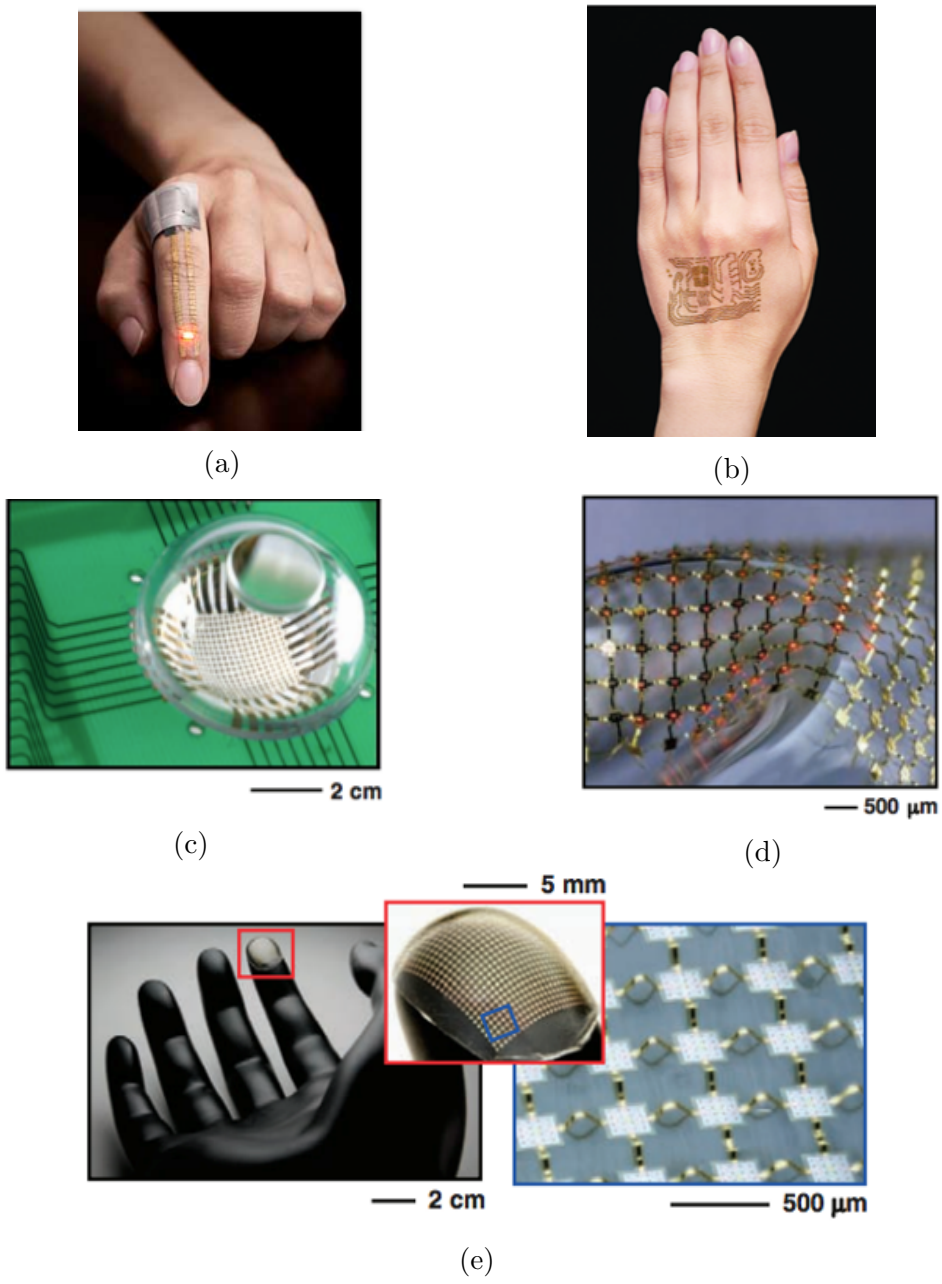


(a) (b) (c) (d) (e)

Figure 1: Uses of Nanomesh: (a) A breathable electronic skin [27] and (b) Conductor created by gold nanomesh [27], (c) Electronic eyeball camera [31], (d) Stretchable LED display instruments that use mesh patterns with micro-scale inorganic Light-emitting diodes [31] and (e) Stretchable silicon circuit with a mesh pattern (left), wrapped onto a structure of a fingertip, presented at low (left), medium (center) and high (right) magnification [31].

pared under same conditions as same areal coverage, cross-sectional area, in-plane contour length and electrical impedance among various inter-connectors in a study. These three different interconnects are named regular serpentine, self-similar serpentine and Archimedean spiral. The disfigured state at the critical strain and released situation while the tension is withdrawn are presented for the three types of spirals. The Archimedean spiral structure

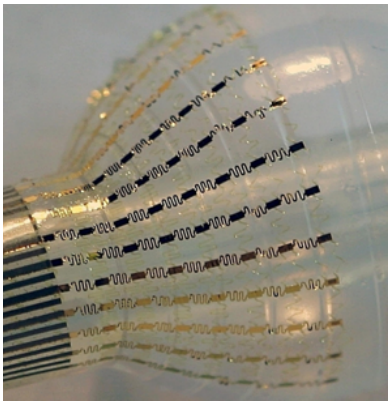

(a)

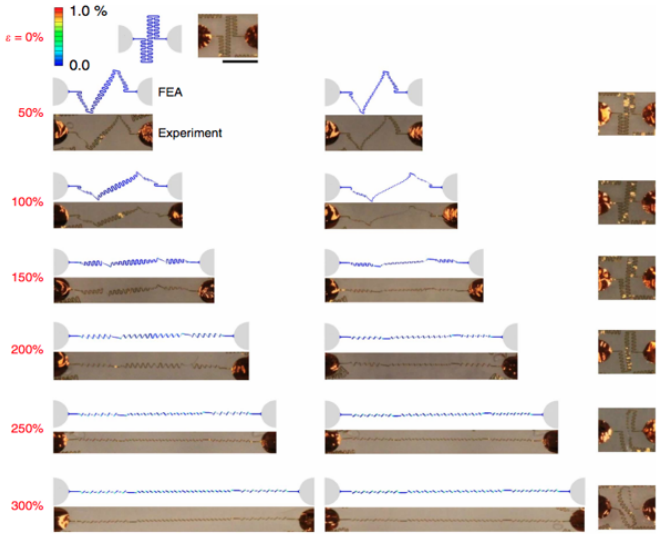


(b)

Figure 2: Self-similar Serpentine Inter-connectors: (a) Non-coplanar serpentine wires on fully inflated balloon of cardiac machine [39] and (b) Deformation of self-similar serpentine wires for various levels of applied tensile strain [43]

can deform out-of-plane largely while the outer ring of the spiral minimizes the in-plane tension by rotation. But, in the Archimedean spiral the horizontal span and vertical span are in little gap, so two spirals have been used to fill in a non-square area. That's why a modified Archimedean spiral structure is proposed by adjusting the ratio between the horizontal and vertical dimensions to make the spiral-based structure to fit in non-square area. The modified Archimedean spiral design can show over 250% elastic stretchability and 325% stretchability before fracture than the original spiral design. The newly added straight portions helped this modified model to gain more stretchability by making the structure to generate out-of-plane deformation with low curvatures. It's also claimed that a uniform and small curvature can increase stretchability largely and the non-periodic pattern is suitable for more degree of freedom instead of periodic pattern for any critical situation [25].

The optimum design, stretchability and the post buckling behavior of order-2 self-similar

serpentine interconnects (SSI) are also studied which are mounted on the polydimethylsiloxane (PDMS) substrate in stretchable electronics. Theoretical modeling, finite element analysis (FEA), and experimental procedures are presented for this study. The scale law is generated through FEM to determine the stretchability as well as the maximum strain of order-2 SSI by using the key geometry parameters like height by space ratio, the proportion of order-2 space to order-1 space, width by space ratio, thickness by space ratio, yield strain. At the time of lateral post buckling, the occurred out-of-plane and in-plane flexural strains are proportionate with the thickness and width of the order-2 SSI, respectively. The FEA results match properly with the experimental results of the deformation modes below 10, 20, 30, and 40% strains. So, the results of stretchablility of the microstructure with order-2 SSI mounted on the PDMS substrate as interconnectors in stretchable electronics got validated through comparing the theoretical formulations, FEM, and experimental results which will be helpful for future development in stretchable electronics, to acquire high stretchability. [12]

The mechanical behavior of the deformation of the polyimide (PI)/metal/PI sandwich serpentine interconnectors with strain-isolating films are also studied under tension loading to gain high elastic stretchability. 3-D numerical simulations are performed to simulate the deformation modes along with strain/stress distributions of the system and then a theoretical simplified 1-D model is developed in a study. These models were used to get the most suitable design along with the material properties and important geometric parameters. The elastic stretchability of this system in Finite element analysis (FEA) was calculated from regular strain formula of deflection per length and in theoretical analysis, the membrane strain along the applied loading direction was calculated with a newly generated formula. The materials of the isolation layer studied here include a silicone elastomer, a biocompatible skin adhesive, a silicone with a modified formulation, and a polydimethylsiloxane. The materials of the substrate include the human skin, the Eco flex and the PDMS here. Three deformation behaviors of the sandwich serpentine models, which includes planar bending, local wrinkling and global buckling, are also discussed here. Planar bending is the least expected deformation case as its deformations are limited and has less stretchability. But, to attain large deflection and low local stress density, global buckling case can provide better stretchabilty than wrinkling mode. A 1-D model was used to create a relationship between the structural factors and the wrinkling wavelength. The proposed simple design system for the strain-isolating films suggests a shift from local wrinkling to global buckling through analysis of the wrinkling wavelengths. It is also extremely effective at differentiating the three deformation modes. The transition point found from FEA results was so close with the wavelengths determined by the analytical results and so the results of normalized wavelengths from the theoretical and FEA results will be so helpful for the evaluation of the sandwich serpentine interconnects to work as highly stretchable functioning devices for more complicated situations [47].

A unified system assembling serpentine interconnectors with toothed substrates of PDMS (10:1 with curing agent) is established to develop the stretchability of the serpentine interconnectors. Both analytical models and numerical simulations are used to establish the stretchability of this integrated system and it seems that the strecthability of serpentine interconnectors with toothed substrate is four times than planar substrate. But, the change of the alignment in-between the serpentine inter-connectors and the toothed substrates effects the

stretchability and the alignment is inversely proportional with stretchability. This deviation is studied by FEA to keep it in an acceptable range. Some analysis are presented on the geometric design of the serpentine inter-connectors also. Those were, the arc angle needs to be a bit smaller compared to the critical arc angle and the thickness of polyimide (PI) needs to be bigger than a critical thickness, otherwise the freely standing serpentine inter-connectors and substrates may get collapsed. The fatigue cracks generated from plastic deformation on arc segments after 25000 times of cycle are analyzed and micro cracks are seen on the interconnects of planar substrate due to less stretchability. So, it's been found that the developed optimal design of the serpentine inter-connectors and toothed substrates system provide larger strechability. [46].

Experimental measurement along with uniaxial tension test is also performed on stretch ability of serpentine thin layers of indium tin oxide (ITO) mounted on kapton with in situ electrical impedance parameters. Effects of different serpentine shapes (basic, U-shaped, horseshoe-shaped, V-shaped), different widths, arm lengths, arc radii, and arc angles on the stretchability of serpentine ITO thin films mounted on Kapton have been tested experimentally and modeled by FEM. The narrower serpentine ribbons of width-to-radius(w/r) ratio lower than 0.4 showed more stretchability than their wider counterparts and as w/r decreased the strain-to-fracture always increased. The arc angle has some non-monotonic effects on serpentine stretchability while the arm length essentially has no influence. Defects or channel cracks in the film also effect less on the overall resistance of the ribbons. The strains-to-fracture determined by crack density was compared with electrical impedance to show that impedance measurement can represent the cracking status in serpentine film. Semi in situ scanning electron microscope (SEM) stretching test is conducted to observe the relation between crack intensity with applied strain and it's found that the cracks got initiated from the inner side of the peak of the serpentines when uni-axial tension was applied on Kapton-bonded serpentine ribbons. This observation was validated by FEM and it is found from the strain distribution that the strain concentration always occurs at the inner side of the peak of the arc, which matches well with the experimental findings. The film gets totally collapsed and no more conductive beyond the critical stretchability. It is determined by experimentally from resistance versus applied strain curve and also by FEM results. A hypothesis that the maximum strain in the serpentine thin film is dependent to a unit-less parameter, explained the experimental and FEM findings and its empirical equation was derived by fitting FEM results [44].

It is now possible to create stretchy electronics that function as well as traditional wafer-based devices. Numerous new uses are made conceivable, ranging from wearable electronics to bio-integrated medicinal devices to electronic eye cams. In terms of the two primary types of stretchy designs, one such example is a wavy pattern that can offer one-dimensional stretchability. The other may be extended in any direction and uses an island-bridge design. For these two designs, mechanics models and comparisons and finite element simulations are examined. The outcomes offer specifications for creating stretchy electronics [38].

Another route to high-performance stretchy electronics is achieved by integrating deformable interconnects with inorganic functional materials. The effect of the substrates made of elastomers on the stretchability of serpentine inter-connectors is theoretically and empirically for a variety of applications examined. From FEA low-cycle fatigue studies, which focus at the stretching needed to create fatigue fractures linked to plastic deformation, support

this trend by revealing a significant improvement in elastic stretchability with decreasing substrate thickness .The FEA simulation predicts that, below a threshold thickness of the substrate, the buckling mode would switch from local wrinkling to global buckling which is confirmed by scanning electron microscopy and 3D optical profiling. Global buckling in thin substrates allows for significant stretching before the serpentine traces flex plastically, greatly increasing the stretchability of these systems [28].

### 1.1.2 Objectives

There are three regular tessellations are available: those that involve packing the 2D plane entirely with equilateral (regular) triangles, squares, or hexagons. The mechanical characteristics of hexagonal nanomesh structures constructed of serpentine traces in the shape of arcs are examined in this thesis to develop a immensely stretchable structure. To explore the displacement, maximum strain, axial stiffness, stretching rigidity, effective modulus, and stretchability of the hexagonal nanomesh structures for various trace thicknesses and arc angles, both theoretical and finite element models are established. The results of the finite element analysis appear to match the analytical results fairly closely. Therefore, these theoretical formulations that have been proven to be correct can be used to have design instructions for building nanomesh structures that have extremely high stretchability and mechanical qualities—two attributes that are highly desirable when creating wearable electronics and bio-inspired structures.

## 1.2 Background Information

### 1.2.1 Elastic Modulus

The elasticity of a material is determined by its modulus of elasticity, commonly referred to as elastic modulus or simply modulus. A material's resistance to elastic, or non-permanent, deformation is measured by its elastic modulus. Materials first have elastic qualities when under stress; the stress causes them to deform, but if the stress is removed, the material will revert to its original state. Materials enter the plastic zone, where they exhibit permanent deformation even after the tensile tension is released, after passing through the elastic region and past their yield point. With an emphasis on the elastic region, the modulus is the result of dividing the stress change by the strain change

$$E = \frac{\text{stress}}{\text{strain}}$$

where strain is the deformation of the material divided by its initial length and stress is force divided by the cross-sectional area of the specimen. Modulus is a constant material characteristic that may be compared between specimens of various sizes. The modulus of a large gold specimen will be the same as a small gold specimen, but the large specimen will need a greater maximum force to deform it. [9] [7]

### 1.2.2 Stiffness of Material

Stiffness is the substance's capacity to withstand external loads and take on its original shape.It's the ability to resist the deformation. Stiffness and elasticity are strongly connected.

A substance has less stiffness the more elastic it is. The amount of deflection generated by the load on the material is measured as the stiffness of the material. The stiffness, K of a body is defined as

$$K = \frac{F}{\Delta}$$

where, F is the force on the body and $\Delta$ is the displacement created by the force along the force's direction. It can also be expressed using Elastic Modulus (E) [5]. There are two types stiffness depending on the direction of applied load.

**Axial Stiffness**

The ratio between axial load and deflection is known as axial stiffness (A.S.). A force exerted parallel to the axis of an object results in an axial load. The axial stiffness can also be expressed as

$$A.S. = \frac{EA}{L}$$

where E is the elastic modulus, A is the cross-section area and L is the length of the material along the force's direction [6].

**Bending Stiffness**

A thin structural element that is subjected to an external load that is imposed perpendicular to the element's longitudinal axis will behave in a way known as bending or flexure [10].The resistance of a member to bending deformation or the moment required to create unit rotation is known as bending stiffness (B.S.). It depends on the Elastic modulus, E, second moment of area, I, and length,L [10]. It can be written as

$$B.S. = \frac{EI}{L}$$

### 1.2.3 Stretching Rigidity

The stretching or axial rigidity (EA) is axial force per applied strain ($\epsilon_{app}$) [8], which can be written as,

$$EA = \frac{Force}{\epsilon_{app}}$$

Any combination of loads can cause a body to deflect elastically, and the deflection at any location in any direction is equal to the partial derivative of strain energy.

### 1.2.4 Nanomesh Structures

Mesh is a type of structure constructed of interconnected strands of flexible or pliable materials, such as metal, fiber, or other. Because a mesh has numerous linked or woven strands, it resembles a web or a net. The mesh structure of nano size is known as nanomesh like

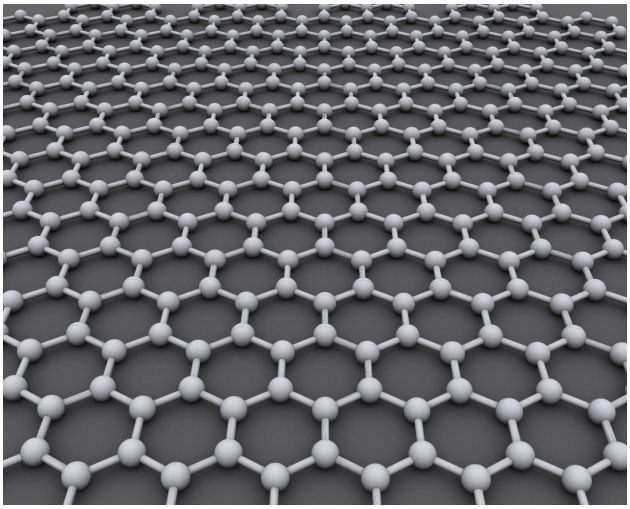

Figure 3: Hexagonal nanomesh structures of Graphene made of carbon atoms [3]

graphene (Figure 3). The mesh structure can be formed in different shapes having triangular, square, rectangular, hexagonal and circular holes etc.

### 1.2.5 Finite Element Analysis

A common technique for numerically resolving differential equations that appear in engineering and mathematical modeling is the finite element method (FEM). The FEM divides a big complex structure into smaller, easier-to-understand components known as finite elements. This is done by creating a mesh of the object. Typically, Finite Element Analysis (FEA) is performed in adopting the techniques of FEM to address actual engineering challenges [23] [26]. There are so many softwares available to perform FEA like Agros2D, DIANA FEA, FEATool Multiphysics, Mathematica, MATLAB, Abaqus, ANSYS, COMSOL Multiphysics etc. Here, in our thesis ABAQUS [37] is used to simulate the structures to find the desired mechanical properties.

# CHAPTER II

## Analytical Approach to Calculate the Mechanical Properties of the Hexagonal Nanomesh Structure

### 2.1 Unit Cell

The schematic diagram of a part of large structure of hexagonal nanomeshes is shown in Figure 4a which is interconnected with arc-shaped serpentine beams. The part of a hexagonal nanomesh shown in Figure 4b is considered as the unit cell of the large hexagonal nanomesh structure. The unit cell consists of one horizontal arc-shaped serpentine trace BD and two inclined arc-shaped serpentine traces AB and BC. The length of a trace is L, half arc-angle $\theta_0$ and the in-plane trace width is t as shown in Figure 4b

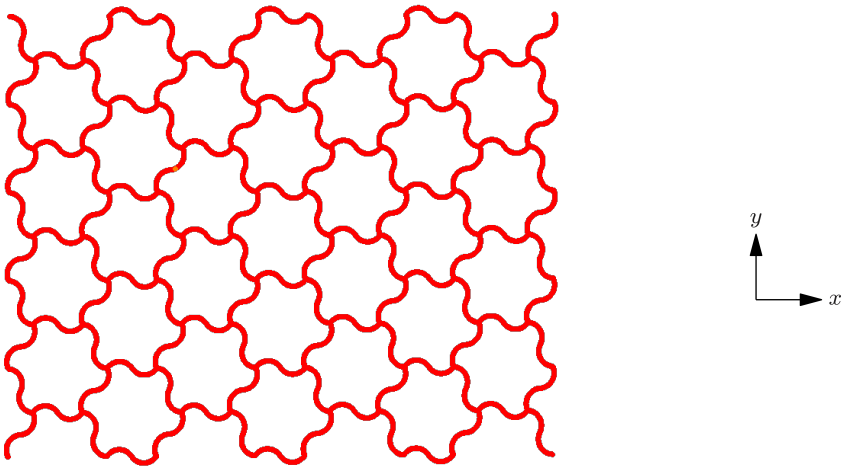


(a)

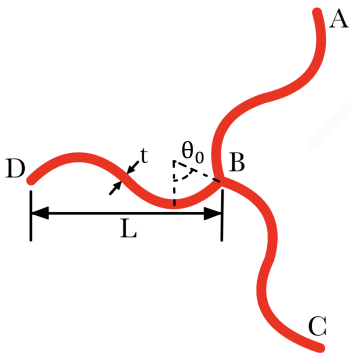


(b)

Figure 4: (a) Arc-shaped serpentine hexagonal nanomesh and (b) Unit cell

The mechanical properties of the hexagonal nanomeshes vary with the direction of the stretching. The structure as well as the unit cell is stretched in both x and y directions to calculate the effective modulus, mechanical stiffness and stretchability using FEA and theoretical approach.

### 2.2 Stretching of Hexagonal Nanomeshes in the x-direction

To find the desired mechanical properties of the hexagonal nanomeshes theoretically along the x-direction, the unit cell is stretched in the x-direction as shown in Figure 5a. The deformed unit cell consists of two inclined beams $A'B'$ and $B'C'$ and one horizontal beam $B'D'$. The internal force analysis of the unit cell for inclined trace and horizontal trace is shown in Figure 5a and Figure 5b respectively.

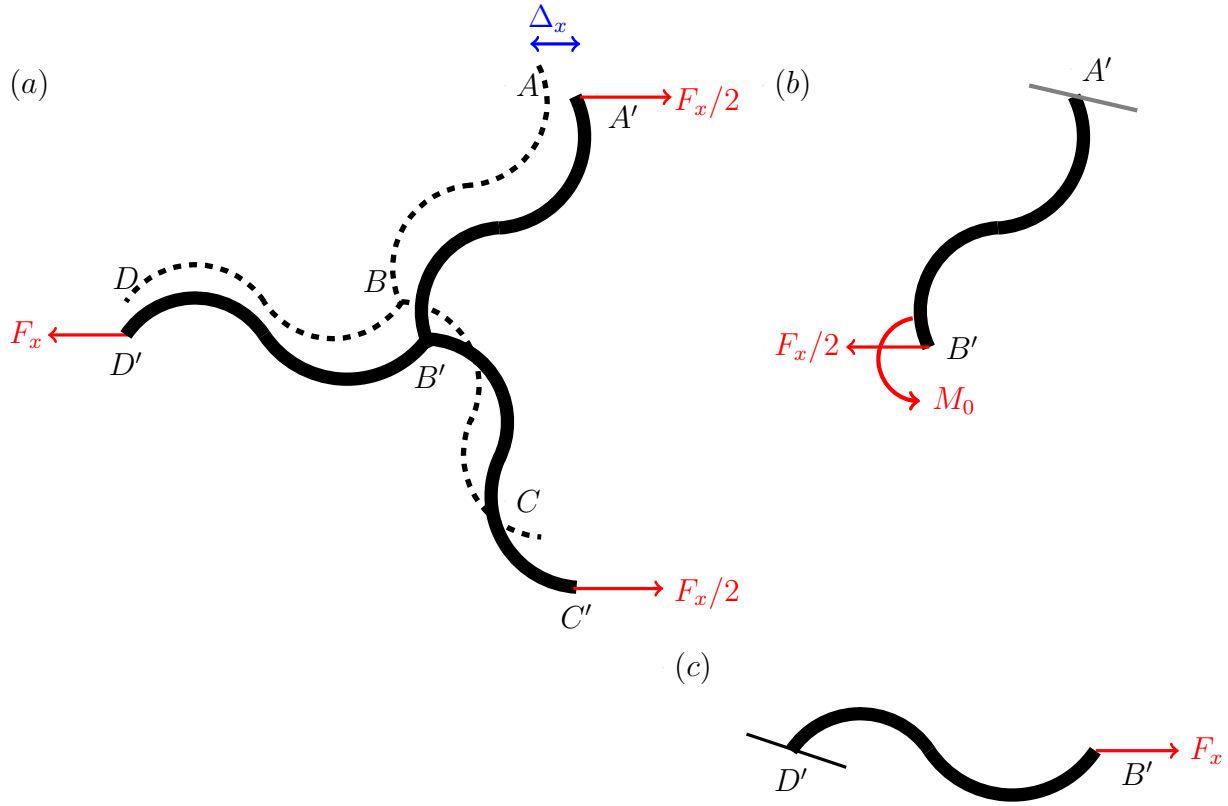


Figure 5: Stretching of the mechanical model of arc-shaped serpentine hexagonal nanomesh in x-direction: (a) Undeformed (dashed lines) and deformed (solid lines) structure of the unit cell,(b) force analysis of the inclined trace and (b) force analysis of the horizontal trace

#### 2.2.1 Displacement of the Inclined Trace

Due to stretching, the axial and transverse shear forces for the inclined beam $A'B'$ (Figure5b) are P and Q respectively as shown in Figure 6a where

$$P = \frac{F_x}{2} \cos\ 60^\circ \tag{2.2.1}$$

$$Q = \frac{F_x}{2} \cos\ 30^\circ \tag{2.2.2}$$

and the reaction moment is $M_0$.

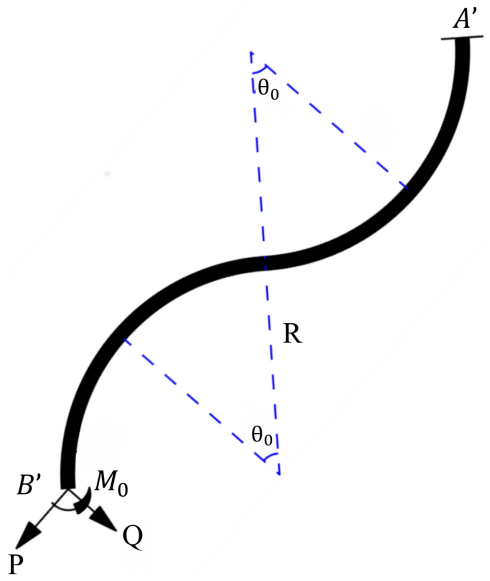


(a)

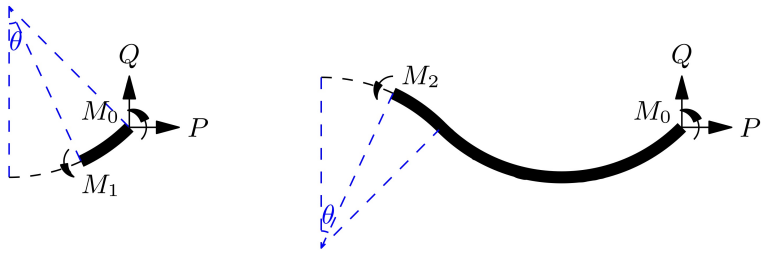


(b)

Figure 6: (a) Force analysis of inclined trace and (b) virtual cut on the trace

Here, for the inclined trace (Figure 6)

$$M_1 = -M_0 - QR\left(\sin\theta_0 - \sin\theta\right) + PR\left(\cos\theta - \cos\theta_0\right) \tag{2.2.3}$$

$$M_2 = -M_0 - QR\left(3\sin\theta_0 - \sin\theta\right) - PR\left(\cos\theta - \cos\theta_0\right) \tag{2.2.4}$$

Using the concept of Strain Energy and Castigliano's Theorem [30],

1. Displacements due to the $P$ force:

$$\begin{aligned}\delta_{1x} &= \int_{-\theta_0}^{\theta_0} \frac{M_1}{EI}\frac{\partial M_1}{\partial P} Rd\theta + \int_{-\theta_0}^{\theta_0} \frac{M_2}{EI}\frac{\partial M_2}{\partial P} Rd\theta \\ &= 2\int_{-\theta_0}^{\theta_0} \frac{PR\left(\cos\theta - \cos\theta_0\right)}{EI} R\left(\cos\theta - \cos\theta_0\right) Rd\theta\end{aligned}$$

$$= \frac{4PR^3}{EI}\left(\theta_0 + \frac{\theta_0 \cos 2\theta_0}{2} - \frac{3\sin 2\theta_0}{4}\right) \tag{2.2.5}$$

$$\delta_{1y} = \int_{-\theta_0}^{\theta_0} \frac{M_1}{EI}\frac{\partial M_1}{\partial Q} R d\theta + \int_{-\theta_0}^{\theta_0} \frac{M_2}{EI}\frac{\partial M_2}{\partial Q} R d\theta$$

$$= \frac{-PR^3}{EI}\left(-4\sin^2\theta_0 + 2\theta_0 \sin 2\theta_0\right) \tag{2.2.6}$$

$$\phi_1 = \int_{-\theta_0}^{\theta_0} \frac{M_1}{EI}\frac{\partial M_1}{\partial M_0} R d\theta + \int_{-\theta_0}^{\theta_0} \frac{M_2}{EI}\frac{\partial M_2}{\partial M_0} R d\theta$$

$$= -\int_{-\theta_0}^{\theta_0} \frac{PR\left(\cos\theta - \cos\theta_0\right)}{EI} R d\theta - \int_{-\theta_0}^{\theta_0} \frac{-PR\left(\cos\theta - \cos\theta_0\right)}{EI} R d\theta$$

$$= 0 \tag{2.2.7}$$

2. Displacements due to the Q force:

$$\delta_{2x} = \int_{-\theta_0}^{\theta_0} \frac{M_1}{EI}\frac{\partial M_1}{\partial P} R d\theta + \int_{-\theta_0}^{\theta_0} \frac{M_2}{EI}\frac{\partial M_2}{\partial P} R d\theta$$

$$= \int_{-\theta_0}^{\theta_0} \frac{-QR\left(\sin\theta_0 - \sin\theta\right)}{EI} R\left(\cos\theta - \cos\theta_0\right) R d\theta - \int_{-\theta_0}^{\theta_0} \frac{-QR\left(3\sin\theta_0 - \sin\theta\right)}{EI} R\left(\cos\theta - \cos\theta_0\right) R d\theta$$

$$= \frac{2QR^3}{EI}\left(2\sin^2\theta_0 - \theta_0 \sin 2\theta_0\right) \tag{2.2.8}$$

$$\delta_{2y} = \int_{-\theta_0}^{\theta_0} \frac{M_1}{EI}\frac{\partial M_1}{\partial Q} R d\theta + \int_{-\theta_0}^{\theta_0} \frac{M_2}{EI}\frac{\partial M_2}{\partial Q} R d\theta$$

$$= -\int_{-\theta_0}^{\theta_0} \frac{-QR\left(\sin\theta_0 - \sin\theta\right)}{EI} R\left(\sin\theta_0 - \sin\theta\right) R d\theta - \int_{-\theta_0}^{\theta_0} \frac{-QR\left(3\sin\theta_0 - \sin\theta\right)}{EI} R\left(3\sin\theta_0 - \sin\theta\right) R d\theta$$

$$= \frac{QR^3}{EI}\left(20\theta_0 \sin^2\theta_0 + 2\theta_0 - \sin 2\theta_0\right) \tag{2.2.9}$$

$$\phi_2 = \int_{-\theta_0}^{\theta_0} \frac{M_1}{EI}\frac{\partial M_1}{\partial M_0} R d\theta + \int_{-\theta_0}^{\theta_0} \frac{M_2}{EI}\frac{\partial M_2}{\partial M_0} R d\theta$$

$$= -\int_{-\theta_0}^{\theta_0} \frac{-QR\left(\sin\theta_0 - \sin\theta\right)}{EI} R d\theta - \int_{-\theta_0}^{\theta_0} \frac{-QR\left(3\sin\theta_0 - \sin\theta\right)}{EI} R d\theta$$

$$= \frac{8QR^2\theta_0 \sin\theta_0}{EI} \tag{2.2.10}$$

3. Displacements due to the $M_0$ force:

$$\delta_{3x} = \int_{-\theta_0}^{\theta_0} \frac{M_1}{EI}\frac{\partial M_1}{\partial P} Rd\theta + \int_{-\theta_0}^{\theta_0} \frac{M_2}{EI}\frac{\partial M_2}{\partial P} Rd\theta$$

$$= \int_{-\theta_0}^{\theta_0} \frac{-M_0}{EI} R\left(\cos\theta - \cos\theta_0\right) Rd\theta - \int_{-\theta_0}^{\theta_0} \frac{-M_0}{EI} R\left(\cos\theta - \cos\theta_0\right) Rd\theta$$

$$= 0 \tag{2.2.11}$$

$$\delta_{3y} = \int_{-\theta_0}^{\theta_0} \frac{M_1}{EI}\frac{\partial M_1}{\partial Q} Rd\theta + \int_{-\theta_0}^{\theta_0} \frac{M_2}{EI}\frac{\partial M_2}{\partial Q} Rd\theta$$

$$= \frac{M_0 R^2}{EI} \int_{-\theta_0}^{\theta_0} \left(4\sin\theta_0 - 2\sin\theta\right) d\theta$$

$$= \frac{8M_0 R^2 \theta_0 \sin\theta_0}{EI} \tag{2.2.12}$$

$$\phi_3 = \int_{-\theta_0}^{\theta_0} \frac{M_1}{EI}\frac{\partial M_1}{\partial M_0} Rd\theta + \int_{-\theta_0}^{\theta_0} \frac{M_2}{EI}\frac{\partial M_2}{\partial M_0} Rd\theta$$

$$= -\int_{-\theta_0}^{\theta_0} \frac{-M_0}{EI} Rd\theta - \int_{-\theta_0}^{\theta_0} \frac{-M_0}{EI} Rd\theta$$

$$= \frac{4M_0 R\theta_0}{EI} \tag{2.2.13}$$

The total displacement of the inclined trace along the x-direction is

$$\delta_x = \delta_{x1} + \delta_{x2} + \delta_{x3} = \frac{4PR^3}{EI}\left(\theta_0 + \frac{\theta_0 \cos 2\theta_0}{2} - \frac{3\sin 2\theta_0}{4}\right) + \frac{2QR^3}{EI}\left(2\sin^2\theta_0 - \theta_0 \sin 2\theta_0\right) \tag{2.2.14}$$

The total rotation of the inclined trace is

$$\phi = \phi_1 + \phi_2 + \phi_3 = \frac{1}{EI}(4RM_0\theta_0 + 0 + 8\theta_0 QR^2 \sin\theta_0) = 0 \tag{2.2.15}$$

So, the bending moment is

$$M_0 = -2QR\sin\theta_0 (CW) \tag{2.2.16}$$

The total displacement of the inclined trace along the y-direction is

$$\delta_y = \frac{R^3}{EI}(4Q\theta_0 \sin^2\theta_0 - P\left(-4sin^2\theta_0 + 2\theta_0 sin\ 2\theta_0\right) + Q(2\theta_0 - sin\ 2\theta_0)) \tag{2.2.17}$$

So, the total displacement of the inclined trace along the x-direction is

$$\Delta_{x1} = \delta_x \ \cos 60^\circ + \delta_y \ \cos 30^\circ$$

$$= \frac{R^3 F_x}{EI}(1.5\theta_0 + \theta_0 \sin^2\theta_0 - \frac{3}{4}\sin 2\theta_0 + \sqrt{3}\sin^2\theta_0 - \frac{\sqrt{3}}{2}\theta_0 \sin 2\theta_0 \qquad (2.2.18)$$

### 2.2.2 Displacement of the Horizontal Trace

For the horizontal trace, the axial force for the horizontal beam $D'B'$ (Figure 5c) is P where,

$$P = F_x \qquad (2.2.19)$$

There is no rotation and no vertical displacement, so, the total rotation is

$$\phi = \phi_1 + \phi_2 + \phi_3 = \frac{1}{EI}(0 + 8QR^2\theta_0 \sin\theta_0 + 4M_0 R\theta_0) = 0$$

or

$$M_0 = -2QR\sin\theta_0 (CW)$$

The total vertical displacement is $\delta_y = \delta_{1y} + \delta_{2y} + \delta_{3y} = 0$ which gives:

$$-PR^3\left(-4\sin^2\theta_0 + 2\theta_0 \sin 2\theta_0\right) + QR^3\left(20\theta_0 \sin^2\theta_0 + 2\theta_0 - \sin 2\theta_0\right) + 8M_0R^2\theta_0 \sin\theta_0 = 0$$

$$Q = P\frac{-4\sin^2\theta_0 + 2\theta_0 \sin 2\theta_0}{4\theta_0 \sin^2\theta_0 + 2\theta_0 - \sin 2\theta_0} \qquad (2.2.20)$$

The total horizontal deflection is therefore:

$$\delta_x = \delta_{1x} + \delta_{2x} + \delta_{3x}$$

or

$$\delta_x = \frac{4PR^3}{EI}\left(\theta_0 + \frac{\theta_0 \cos 2\theta_0}{2} - \frac{3\sin 2\theta_0}{4}\right) + \frac{2QR^3}{EI}\left(2\sin^2\theta_0 - \theta_0 \sin 2\theta_0\right) + 0$$

$$= \frac{4PR^3}{EI\left(4\theta_0 - 2\theta_0 \cos 2\theta_0 - \sin 2\theta_0\right)}\left[3\theta_0^2 - 2\theta_0 \sin 2\theta_0 - 2\cos 2\theta_0 - (1+\theta_0)\sin 4\theta_0 - \frac{7}{8}\cos 4\theta_0 - \frac{9}{8}\right] \qquad (2.2.21)$$

The total displacement of the horizontal trace along the x-direction is

$$\Delta_{x2} = \frac{4FR^3}{EI(4\theta_0 - 2\theta_0 \ cos2\theta_0 - sin2\theta_0)}(3\theta_0^2 - 2\theta_0 \ sin \ 2\theta_0 + 2 \ cos2\theta_0 - \frac{\theta_0 \ sin4\theta_0}{2} - \frac{7}{8}cos4\theta_0 - \frac{9}{8}) \qquad (2.2.22)$$

### 2.2.3 Displacement of the Unit Cell

So, from Eqs.(2.2.18) and (2.2.22) the total displacement of the unit cell along the x-direction is

$$\Delta_x = \Delta_{x1} + \Delta_{x2}$$
$$= \frac{F_x R^3}{EI}\left(\frac{4(3\theta_0^2 - 2\theta_0\ sin\ 2\theta_0 + 2\ cos2\theta_0 - \frac{\theta_0\ sin4\theta_0}{2} - \frac{7}{8}cos4\theta_0 - \frac{9}{8})}{(4\theta_0 - 2\theta_0\ cos2\theta_0 - sin2\theta_0)}\right.$$
$$\left. + (1.5\theta_0 + \theta_0 \sin^2\theta_0 - \frac{3}{4}\sin 2\theta_0 + \sqrt{3}\sin^2\theta_0 - \frac{\sqrt{3}}{2}\theta_0 \sin 2\theta_0)\right) \quad (2.2.23)$$

### 2.2.4 Effective Modulus and Stretchability of the Nanomesh

The axial stiffness of the unit cell is

$$\frac{EA}{\overline{L}} = \frac{F_x}{\Delta_x} \quad (2.2.24)$$

where $E$ is the elastic modulus of the beam, $A$ is the cross-sectional area and $\overline{L}$ is $L(1 + \cos 60^\circ)$ as shown in Figure 7

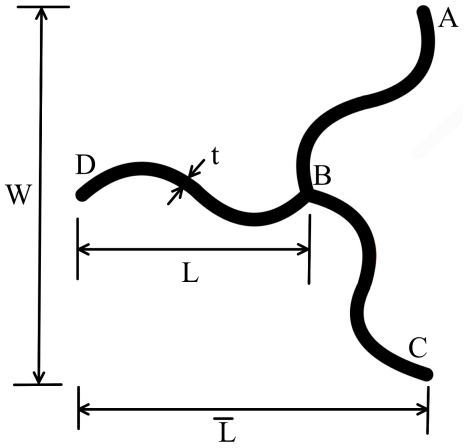


Figure 7: Unit cell dimensions.

The applied strain is

$$\epsilon_{app} = \frac{\Delta_x}{\overline{L}} \quad (2.2.25)$$

The stretching rigidity is

$$\overline{EA} = \frac{F_x}{\epsilon_{app}} \quad (2.2.26)$$

The effective modulus of the nanomesh is

$$E_{x-eff} = \frac{\overline{EA}}{Wh} = \frac{F_x \overline{L}}{\Delta_x W h} \quad (2.2.27)$$

where $W = 2L \sin 60^\circ$.

So,

$$E_{x-eff} = \frac{F_x(1+\cos 60^\circ)}{2\Delta_x h \sin 60^\circ} \tag{2.2.28}$$

Solving Eqs. (2.2.23) and (2.2.28) yields

$$E_{x-eff} = \frac{\sqrt{3}EI}{2hR^3\gamma} \tag{2.2.29}$$

where

$$\gamma = (\frac{4(3\theta_0^2 - 2\theta_0\ sin\ 2\theta_0 + 2\ cos2\theta_0 - \frac{\theta_0\ sin4\theta_0}{2} - \frac{7}{8}cos4\theta_0 - \frac{9}{8})}{(4\theta_0 - 2\theta_0\ cos2\theta_0 - sin2\theta_0)}$$

$$+(1.5\theta_0 + \theta_0 \sin^2\theta_0 - \frac{3}{4}\sin 2\theta_0 + \sqrt{3}\sin^2\theta_0 - \frac{\sqrt{3}}{2}\theta_0 \sin 2\theta_0))$$

There are bending moment $M'$ and $M''$ on the right most end and the peak of the first half of a single trace as shown in Figure 8

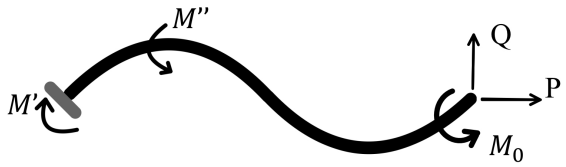


Figure 8: Bending moments on a single trace.

where

$$M'' = -M_0 - PR + PR\cos\theta_0 - 3QR\sin\theta_0 \tag{2.2.30}$$

$$M' = M_0 + 4QR\sin\theta_0 \tag{2.2.31}$$

Here, for stretching the nanomeshes along the x-direction, $M' > M''$

So, the maximum strain in the nanomesh is

$$\epsilon_{xmax} = \frac{M't}{2EI} \tag{2.2.32}$$

Solving Eqs. 2.2.2, 2.2.16, 2.2.23, 2.2.25, 2.2.31 and 2.2.32 yields

$$\frac{\epsilon_{xmax}}{\epsilon_{app}} = \frac{\frac{\frac{\sqrt{3}}{2}F_x R\sin\theta_0 t}{2EI}}{\frac{\Delta_x}{\overline{L}}} = \frac{\sqrt{3}F_x R\sin\theta_0 t\overline{L}}{4EI\Delta_x}$$

$$= \frac{\sqrt{3}\sin\theta_0 tL(1+\cos 60^\circ)}{4R^2\alpha} \tag{2.2.33}$$

where,

$$\alpha = \frac{4(3\theta_0^2 - 2\theta_0\ sin\ 2\theta_0 + 2\ cos2\theta_0 - \frac{\theta_0\ sin4\theta_0}{2} - \frac{7}{8}cos4\theta_0 - \frac{9}{8})}{(4\theta_0 - 2\theta_0\ cos2\theta_0 - sin2\theta_0)}$$

$$+(1.5\theta_0 + \theta_0 \sin^2\theta_0 - \frac{3}{4}\sin 2\theta_0 + \sqrt{3}\sin^2\theta_0 - \frac{\sqrt{3}}{2}\theta_0 \sin 2\theta_0))$$

and

$$\epsilon_{xmax} = \epsilon_{app}\frac{\sqrt{3}\sin\theta_0 tL(1+\cos 60°)}{4R^2\alpha} \tag{2.2.34}$$

When $\epsilon_{xmax}$ gets equal to the intrinsic fracture strain $\epsilon_f$, the $\epsilon_{app}$ is considered as the stretchability $\epsilon_{xstr}$ of the structure. So, the stretchability of the hexagonal nanomesh structures along the x-direction is

$$\epsilon_{xstr} = \epsilon_f \frac{4R^2\alpha}{\sqrt{3}\sin\theta_0 tL(1+\cos 60°)} \tag{2.2.35}$$

### 2.3 Stretching of Hexagonal Nanomeshes in the y-direction

In this case, the unit cell is stretched along the y-direction as shown in Figure 9. The deformation of the horizontal beam is negligible here. The internal force analysis is shown in Figure 9.

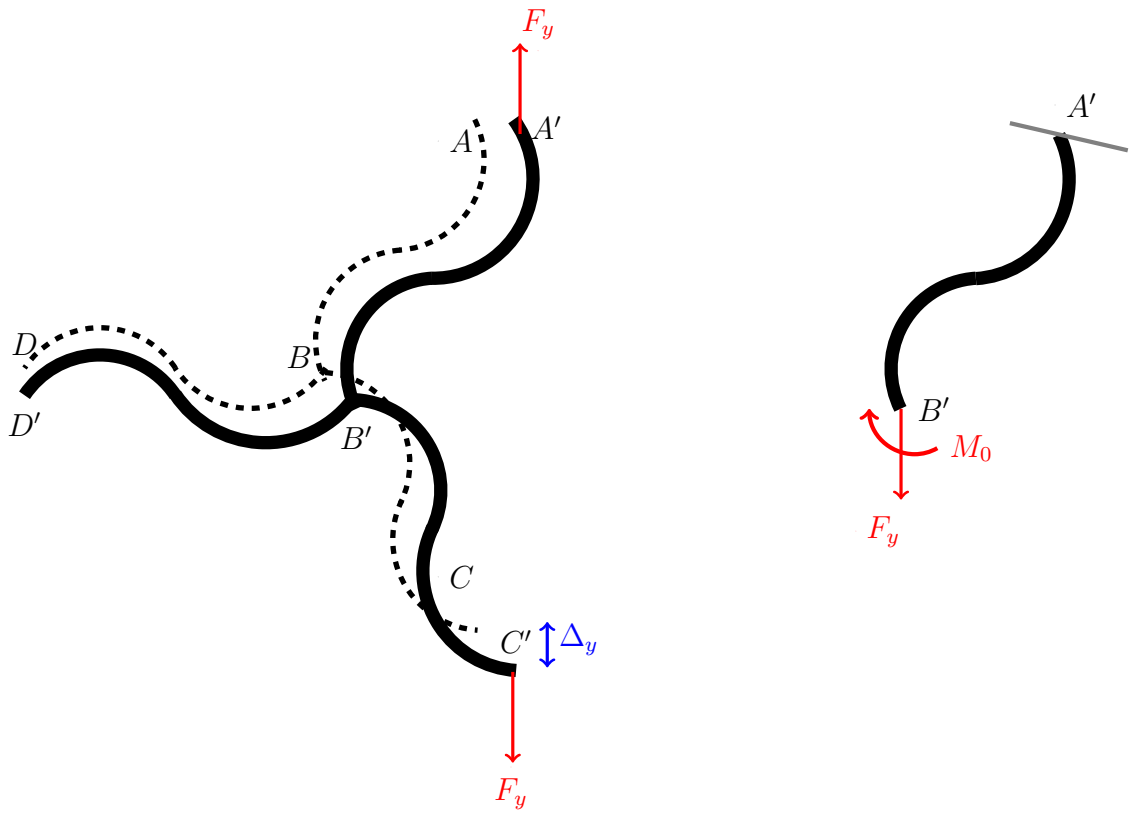


Figure 9: Stretching of the mechanical model of arc-shaped serpentine hexagonal nanomesh in y-direction: (a) Undeformed (dashed lines) and deformed (solid lines) structure of the unit cell,(b) Internal force analysis

### 2.3.1 Displacement of the Unit Cell

The axial and transverse shear forces on the upper inlcined trace due to stretching are as follows:

$$P = F_y \cos\ 30^\circ \tag{2.3.1}$$

$$Q = F_y \sin\ 30^\circ \tag{2.3.2}$$

The axial and transverse shear forces on the lower inlcined trace due to stretching are as follows:

$$P = F_y \cos\ 30^\circ \tag{2.3.3}$$

$$Q = -F_y \sin\ 30^\circ \tag{2.3.4}$$

There is no vertical displacement on the horizontal trace, so, the inclined traces' vertical displacement is the total displacement of the structure in the y-direction which is,

$$\Delta_y = \delta_{y1} + \delta_{y2} = \delta_x\ \cos 30^\circ + \delta_y\ \cos 60^\circ + \delta_x\ \cos 30^\circ - \delta_y\ \cos 60^\circ$$

$$\Delta_y = 2\delta_x\ \cos 30^\circ$$

$$So, \Delta_y = \frac{8PR^3}{EI}(\ \theta_0 + \frac{\theta_0\ \cos\ 2\theta_0}{2} - \frac{3\ \sin 2\theta_0}{4})\cos 30^\circ + \frac{4QR^3}{EI}(2\sin^2\ \theta_0 - \theta_0 \sin\ 2\theta_0)\cos 30^\circ \tag{2.3.5}$$

### 2.3.2 Effective Modulus and Stretchability of the Nanomesh

The axial stiffness of the unit cell is

$$\frac{EA}{\overline{L}} = \frac{F_y}{\Delta_y} \tag{2.3.6}$$

where $E$ is the elastic modulus of the beam, $A$ is the cross-sectional area and $\overline{L}$ is $2L\sin 60^\circ$ as shown in Figure 10

The applied strain is

$$\epsilon_{app} = \frac{\Delta_y}{\overline{L}} \tag{2.3.7}$$

The stretching rigidity is

$$\overline{EA} = \frac{F_y}{\epsilon_{app}} \tag{2.3.8}$$

The effective modulus of the nanomesh is

$$E_{y-eff} = \frac{\overline{EA}}{Wh} = \frac{F_y\overline{L}}{\Delta_y Wh} \tag{2.3.9}$$

where $W = L + L\cos 60^\circ$.

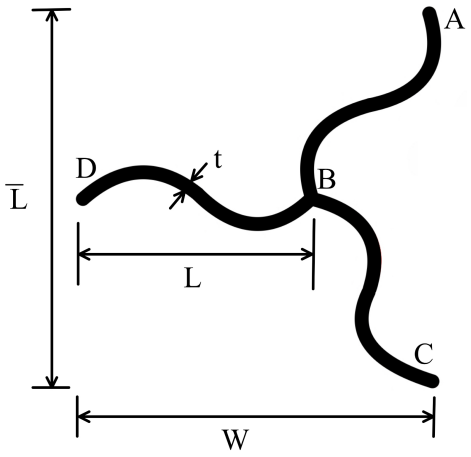

Figure 10: Unit cell dimensions.

So,

$$E_{y-eff} = \frac{2F_y \sin 60^\circ}{\Delta_y h(1+\cos 60^\circ)} \tag{2.3.10}$$

where h= out of plane thickness

Here, for stretching the structure along the y-direction,
for $0^\circ < \theta_0 < 60^\circ$ or $0^\circ < Arc - angle(2\theta_0) < 120^\circ$,

$$|M'| > |M''|$$

and thus,

$$\epsilon_{1ymax} = \frac{M't}{2EI} \tag{2.3.11}$$

Solving Eqs. 2.3.4, 2.2.16, 2.2.31, 2.3.5, 2.3.7 and 2.3.11 yields

$$\begin{aligned}\frac{\epsilon_{1ymax}}{\epsilon_{app}} &= \frac{\frac{F_y R \sin\theta_0 t}{2EI}}{\frac{\Delta_y}{\overline{L}}} \\ &= \frac{F_y R \sin\theta_0 t \overline{L}}{2EI\Delta_y} \\ &= \frac{\sqrt{3}\sin\theta_0 tL}{2R^2\beta}\end{aligned} \tag{2.3.12}$$

where,

$$\beta = (10\theta_0 - 4\theta_0 \sin^2\theta_0 + 4\sqrt{3}\sin^2\theta_0 - 5\sin 2\theta_0 - 2\sqrt{3}\theta_0 \sin 2\theta_0)$$

and

$$\epsilon_{1ymax} = \epsilon_{app}\frac{\sqrt{3}\sin\theta_0 tL}{2R^2\beta} \tag{2.3.13}$$

Similarly, when $\epsilon_{1ymax}$ gets equal to the intrinsic fracture strain $\epsilon_f$, the $\epsilon_{app}$ is considered

as the stretchability $\epsilon_{1ystr}$ of the structure. So, the stretchability of the hexagonal nanomesh structures along the y-direction is

$$\epsilon_{1ystr} = \epsilon_f \frac{2R^2\beta}{\sqrt{3}\sin\theta_0 tL} \tag{2.3.14}$$

for $60^\circ < \theta_0 < 179.5^\circ$ or $120^\circ < Arc - angle(2\theta_0) < 359^\circ$

$$|M''| > |M'|$$

and thus,

$$\epsilon_{2ymax} = \frac{M''t}{2EI} \tag{2.3.15}$$

Solving Eqs. 2.3.4,2.2.16, 2.2.31,2.3.5, 2.3.7 and 2.3.15 yields

$$\frac{\epsilon_{2ymax}}{\epsilon_{app}} = \frac{\sqrt{3}tL}{2R^2\lambda}$$

where,

$$\lambda = \frac{(10\theta_0 - 4\theta_0\sin^2\theta_0 + 4\sqrt{3}\sin^2\theta_0 - 5\sin 2\theta_0 - 2\sqrt{3}\theta_0\sin 2\theta_0)}{\frac{\sqrt{3}}{2}\cos\theta_0 - 0.5\sin\theta_0 - \frac{\sqrt{3}}{2}}$$

and

$$\epsilon_{2ymax} = \epsilon_{app}\frac{\sqrt{3}tL}{2R^2\lambda} \tag{2.3.16}$$

So, the stretchability is

$$\epsilon_{2ystr} = \epsilon_f \frac{2R^2\lambda}{\sqrt{3}tL} \tag{2.3.17}$$

# CHAPTER III

## Finite Element Model of the Hexagonal Nanomesh Structure

### 3.1 Simulation of the Structure

Finite element analysis (FEA) is used to simulate the hexagonal nanomeshes to study its mechanical properties. Here, FEA is conducted with the finite element tool ABAQUS [16].

#### 3.1.1 Create Part

To create the part the modeling space is chosen as 3D as the interconnector beams are three dimensional having length, width and out of plan thickness. The type is selected as deformable and in the base feature, planar and wire is selected as the shape. After drawing the unit cell (Figure 4b) including three arc-shaped serpentine traces, translating tool is used to imitate the unit cell and creating the section sketch of the large nanomesh structure as shown in Figure 11.

The geometric dimensions of the sketch are applied maintaining three $\frac{R}{t}$ ratios 10, 20, 30 and $\frac{L}{t} >= 10$, where R is the arc-radius and t is the trace-width. So, for R= 180nm and h = 5nm, the trace widths are varied as t = 18nm, 9nm and 6nm. For each of the three $\frac{R}{t}$ ratios, the arc-angle of the traces are varied from 22.5° to 135°.

#### 3.1.2 Material and the Properties

Here, the inter-connector beams are considered as thin gold (Au) films. Generally, the electrodes made from gold (Au) nanomesh have better qualities, such as low electrical impedance, higher transparency, good cell survival, and excellent flexibility, than the other materials like indium tin oxide (ITO) and graphene electrodes etc [35]. Gold is also among the best materials to manufacture multi electrode arrays because of its excellent chemical stability, high electrical conductivity, and biocompatibility. Noble metals, such as gold, do not, however, attach to the glass substrate very effectively. Gold films thus become destroyed when exposed to water, placing restrictions on the use of gold thin films as an electrode. So, there are research works on straightforward and economical approach for producing gold electrode arrays [40].

So, here the elastic modulus for the traces is considered as 79GPa which is the Young's modulus of the thin gold strands [24], the material density as $1.93E-235kg/nm^3$, the Poisson's ratio as 0.425 and the shear modulus as 30 GPa.

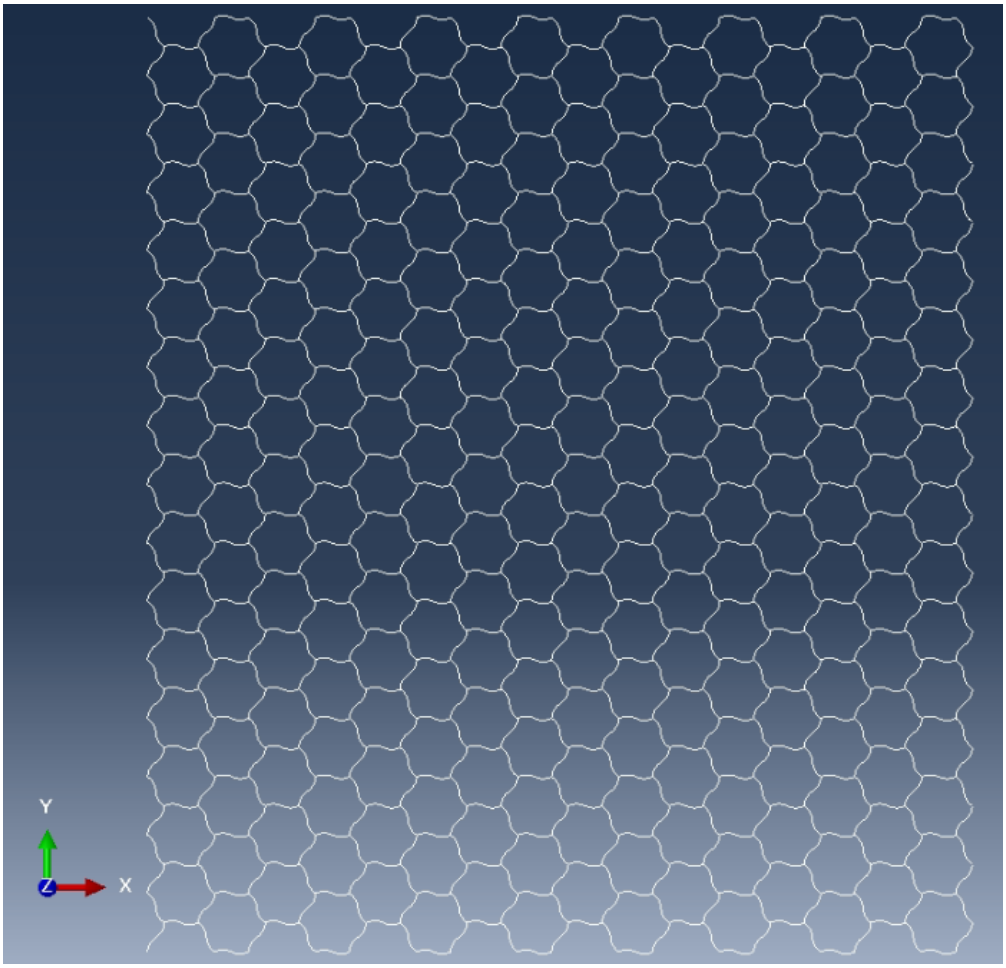

Figure 11: Section Sketch of a 16 by 16 Hexagonal Nanomesh Structure

### 3.1.3 Boundary Conditions

#### Stretching in x-direction

The boundary conditions for the simulation of the stretching of the large hexagonal nanomesh structure along the x-direction is applied on the outer nodes of the structure as shown in Figure 12

The applied strain on the nanomesh structure is $\epsilon_{app} = 10\%$ and so, the value of $\Delta_x$ is provided as $0.1\overline{L}$.

#### Stretching in y-direction

Similary, for the stretching along the y-direction, the boundary conditions are applied on the outer nodes of the structure as shown in Figure 13

The applied strain on the nanomesh structure is $\epsilon_{app} = 10\%$ and so, the value of $\Delta_y$ is provided as $0.1\overline{L}$.

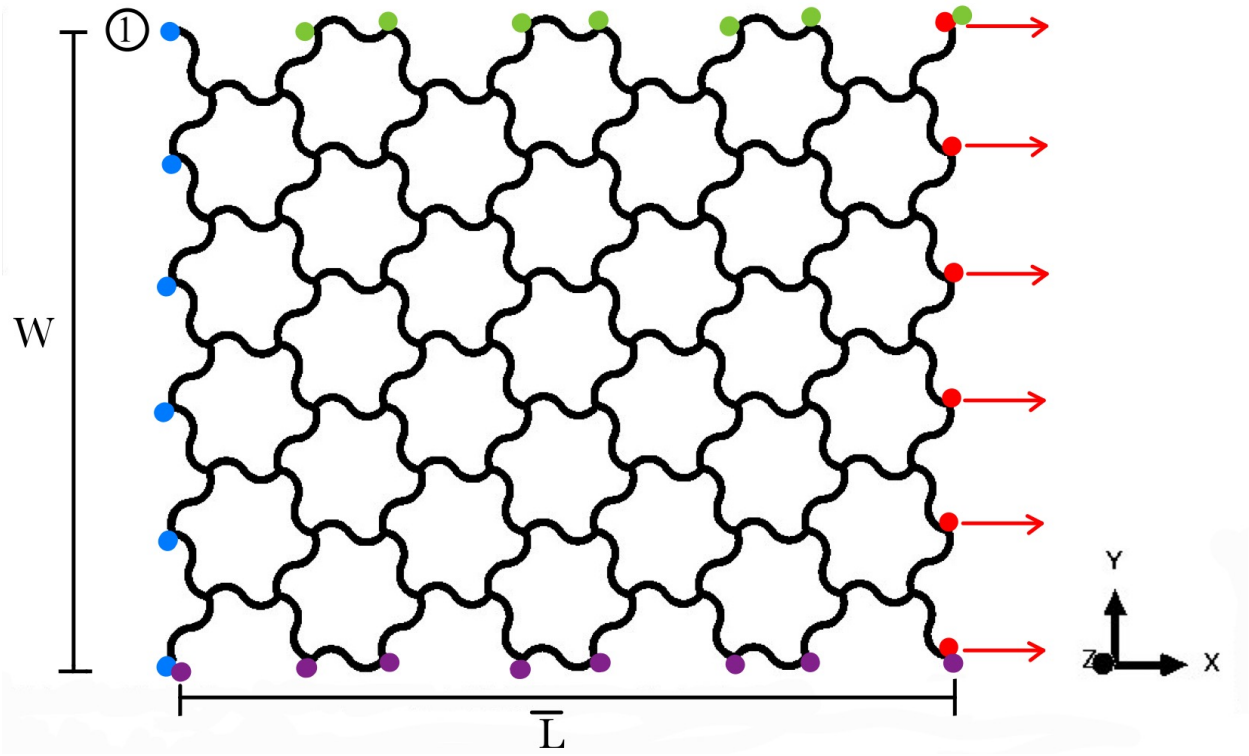


Figure 12: Boundary Conditions on a Part of the Large Hexagonal Nanomesh Structure: Blue nodes: U1=UR3=0, Red nodes: U1=given value of $\Delta_x$, UR3=0, Purple Nodes: U2=UR3=0, Green Nodes: UR3=0, U2 of the green nodes= U2 of node 1, where U1= displacement along the x-axis, U2= displacement along the y-axis, UR3= rotational displacement along the z-axis.

### 3.1.4 Mesh Generation

Here, each trace is meshed into 100 mesh elements as shown in Figure 14. More fine meshing provide better results but cause higher computation time and as the difference in results is negligible, so meshing into 100 elements was an optimum option in every way. The mesh element is chosen as beam element and quadratic in geometric order. Because, the single traces are considered as beam and the quadratic element refers to a quadratic shape function, which indicates that when this kind of element is utilized between two point locations, the deformation along the edge satisfies second order polynomial or quadratic equation ($ax^2 + bx + c$). The linear element follows the linear shape function which allows an element to deform linearly following the linear equation (ax+b). When there is significant deformation, the quadratic element provides a more precise result. [4]

### 3.1.5 Effective Modulus

Due to stretching along the x and y directions there are reaction forces (RF1) generated on the red nodes of Figure 12 and Figure 13. The reaction forces generated in FEA simulation is shown in Figure 15.

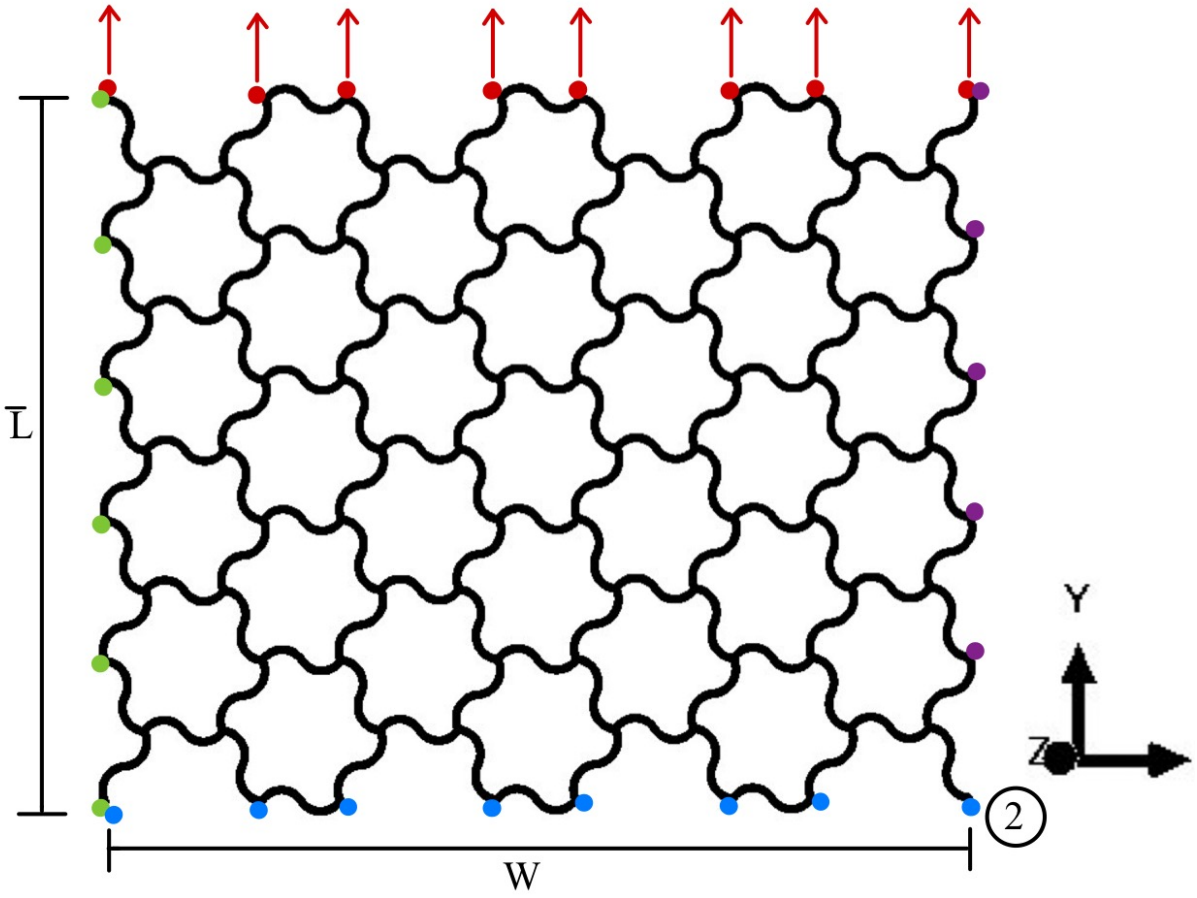


Figure 13: Boundary Conditions on a Part of the Large Hexagonal Nanomesh Structure: Blue nodes: U2=UR3=0, Red nodes: U2=given value of $\Delta_y$, UR3=0, Purple Nodes: UR3=0, U1 of the Purple Nodes = U1 of Node2 Green Nodes: U1=UR3=0, U1= displacement along the x-axis, U2= displacement along the y-axis, UR3= rotational displacement along the z-axis.

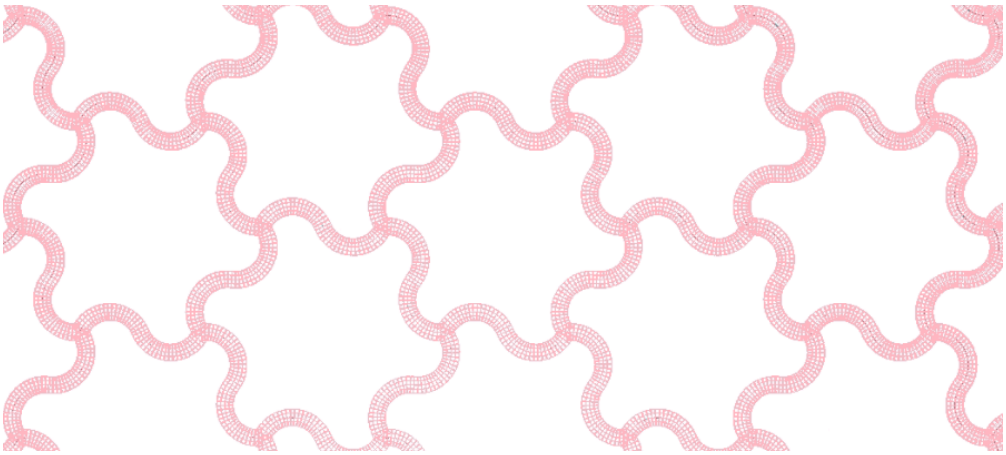

Figure 14: Mesh Generation

Finally, the effective modulus of the nanomesh structure is calculated as

$$E_{eff} = \frac{\sum RF_1 \overline{L}}{W \Delta h} \tag{3.1.1}$$

where $\sum RF_1$ is the summation of the reaction forces on red nodes, $\overline{L}$ is the length of the nanomesh structure along the stretching direction and W is the width of the nanomesh strcuture as shown in Figure 12 and Figure 13.

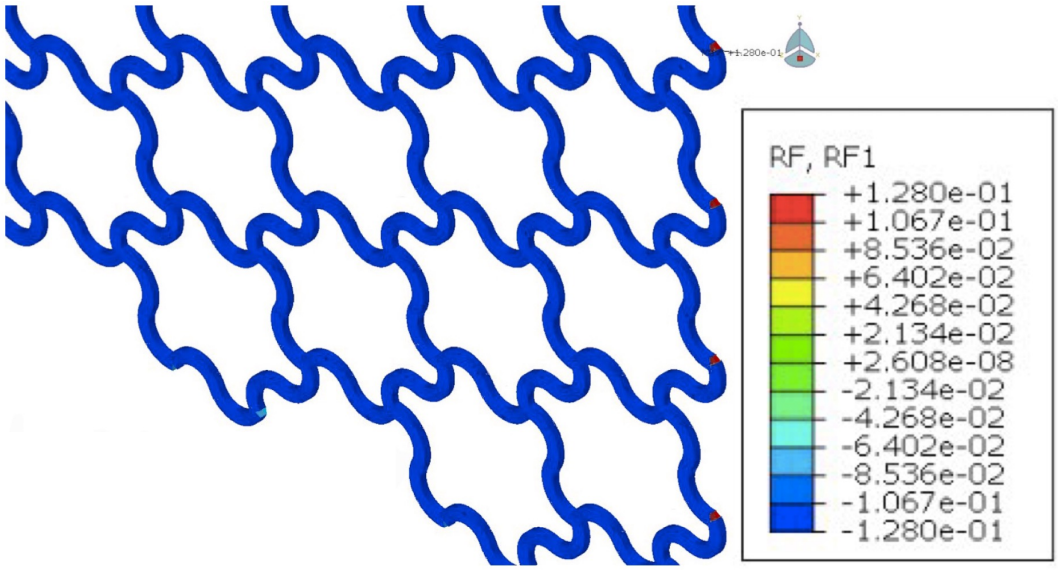


Figure 15: Reaction forces generated due to stretching in the x-direction

# CHAPTER IV

## Effective Moduli and Stretchability of the Nanomesh Structure for Different Geometric Parameters

### 4.1 Effective Moduli due to Stretching in the x-direction

The effective moduli due to stretching the nanomesh along the x-direction is calculated by FEA using the similar procedure as in the analytical model. The Eq. 3.1.1 is used in FEA to find the effective modulus for different geometrical parameters of the structure. The theoretical results along with a few corresponding FEA results for the effective moduli of the nanomeshes for three $\frac{R}{t}$ ratios and the arc-angles 22.5°to 153°are plotted in Figure 16. The theoretical findings are in excellent agreement with the FEA findings as shown for the arc-angle 36°, 54°and 112.5°and 135°for three different $\frac{R}{t}$ ratios. The theoretical presumptions therefore match the FEA results quite well.

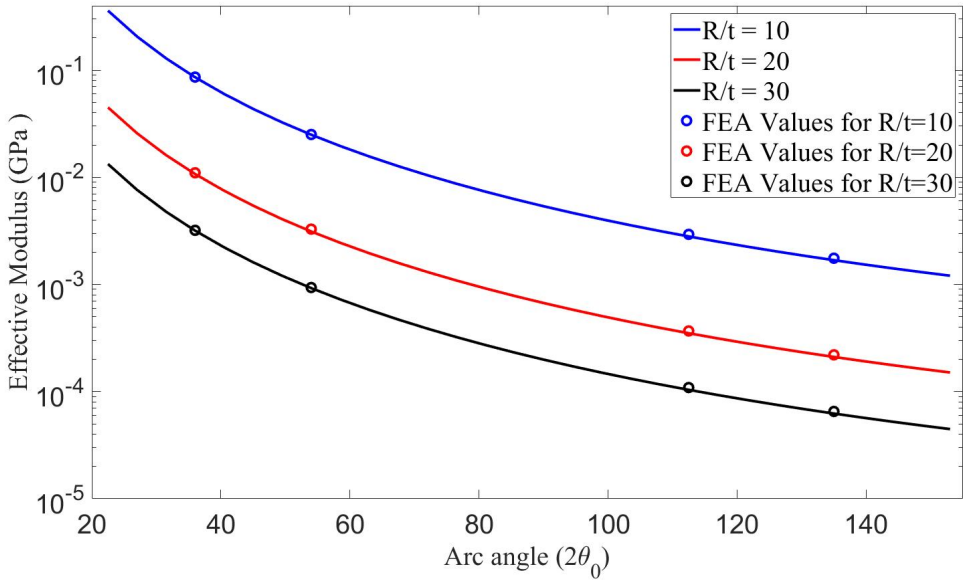


Figure 16: Effective moduli($E_{x-eff}$) of the nanomeshes versus arc angle ($2\theta_0$)

The normalized effective modulus is the effective modulus of the nanomeshes divided by 79 GPa which is the elastic modulus of the ultra-thin gold film [24]. The variation of normalized effective modulus with arc-angle for different $\frac{R}{t}$ ratios are plotted in Figure 17.

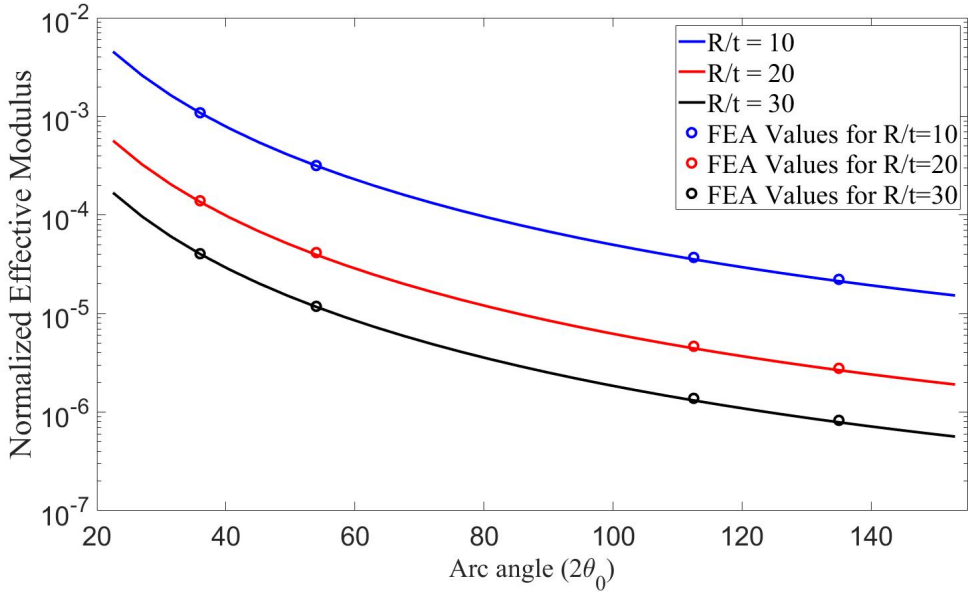


Figure 17: Normalized effective modulus ($\frac{E_{x-eff}}{E}$) versus arc angle ($2\theta_0$)

### 4.2 Effective Moduli due to Stretching in the y-direction

The effective moduli due to stretching the nanomesh along the y-direction is calculated by FEA adopting the similar concept as in the analytical model. The Eq. 3.1.1 is used in FEA to find the effective modulus for different geometrical parameters of the structure. The theoretical results along with a few corresponding FEA results for the effective moduli of the nanomeshes for three $\frac{R}{t}$ ratios and the arc-angles 22.5°to 153°are plotted in Figure 18. The theoretical findings are in good agreement with the FEA findings as shown for the arc-angle 36°, 54°and 112.5°and 135°for three different $\frac{R}{t}$ ratios. The theoretical predictions therefore match the FEA results pretty well.

### 4.3 Maximum Strain and Stretchability along the x-Direction

The maximum strain of the nanomesh structures due to stretching along the x-direction are calculated using the expressions from section 2.2 for 10% applied strain. The FEA and theoretical calculations follow similar conditions and procedures. The FEA results of deformation and strain distribution are presented in Figure 20 and Figure 21 for the arc-angles 112 °and 135°. The maximum strain of the hexagonal nanomeshes are plotted in Figure 22 for the three $\frac{R}{t}$ ratios and the arc-angles 22.5°to 153°. For the arc-angles 36°, 54°, 112.5°and 135°, the theoretical results agree quite closely with the FEA results. Therefore, it can be claimed that the theoretical presumptions and the FEA results are in good agreement.

In Figure 23, plots for three distinct $\frac{R}{t}$ ratios and the arc-angles 22.5°to 153°represent the normalized stretchability of the structures, which is the ratio of applied strain to intrinsic fracture strain of the traces.

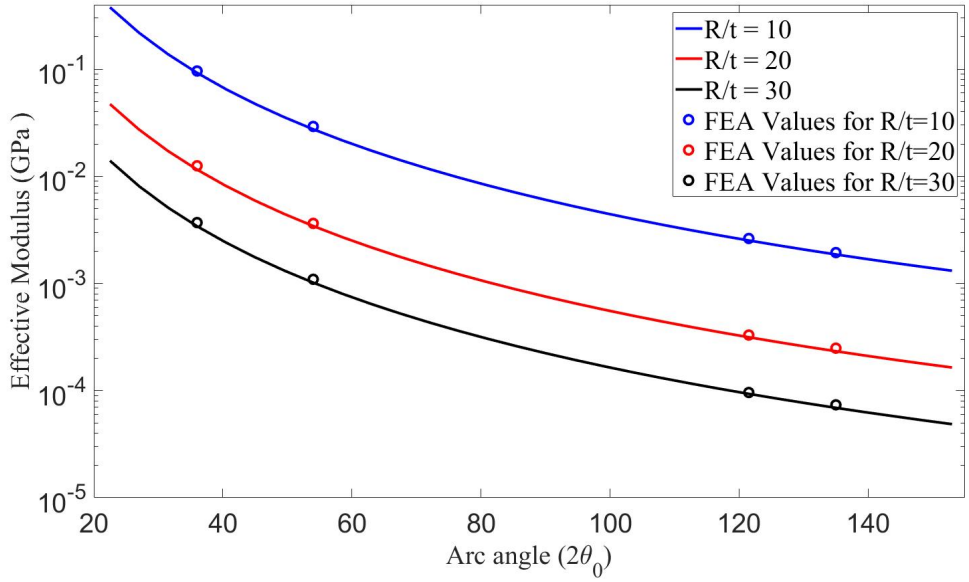


Figure 18: Effective moduli($E_{y-eff}$) of the nanomeshes versus arc angle ($2\theta_0$)

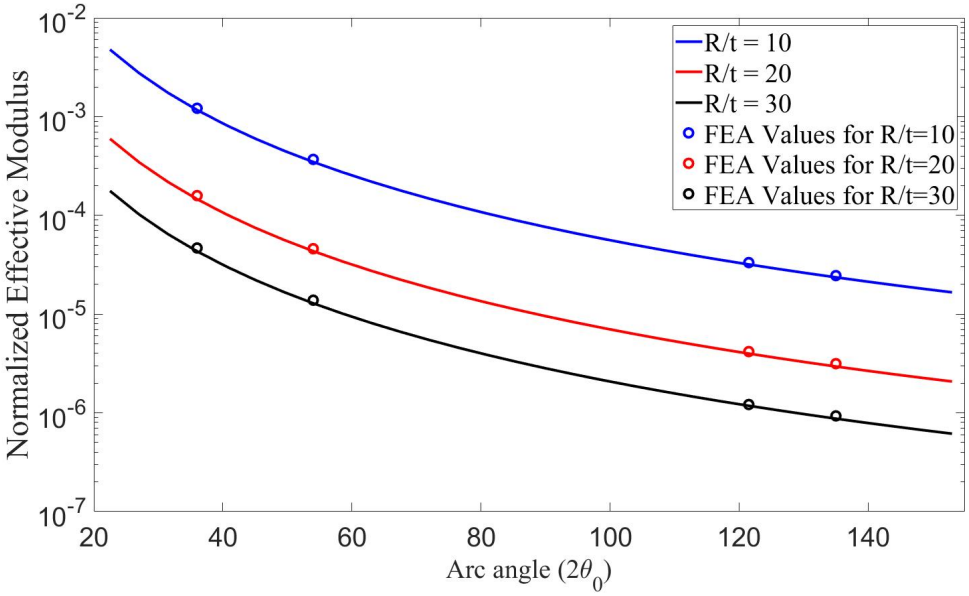


Figure 19: Normalized effective modulus ($\frac{E_{y-eff}}{E}$) versus arc angle ($2\theta_0$)

### 4.4 Maximum Strain and Stretchability along the y-Direction

The maximum strain of the nanomesh structures due to stretching along the y-direction are calculated using the expressions from section 2.3 for 10% applied strain. The FEA and theoretical calculations follow similar steps and boundary conditions. The maximum strain of the hexagonal nanomeshes are plotted in Figure 24 for the three $\frac{R}{t}$ ratios and the arc-angles 22.5°to 153°. For the arc-angles 36°, 54°, 112.5°and 135°, the theoretical results agree

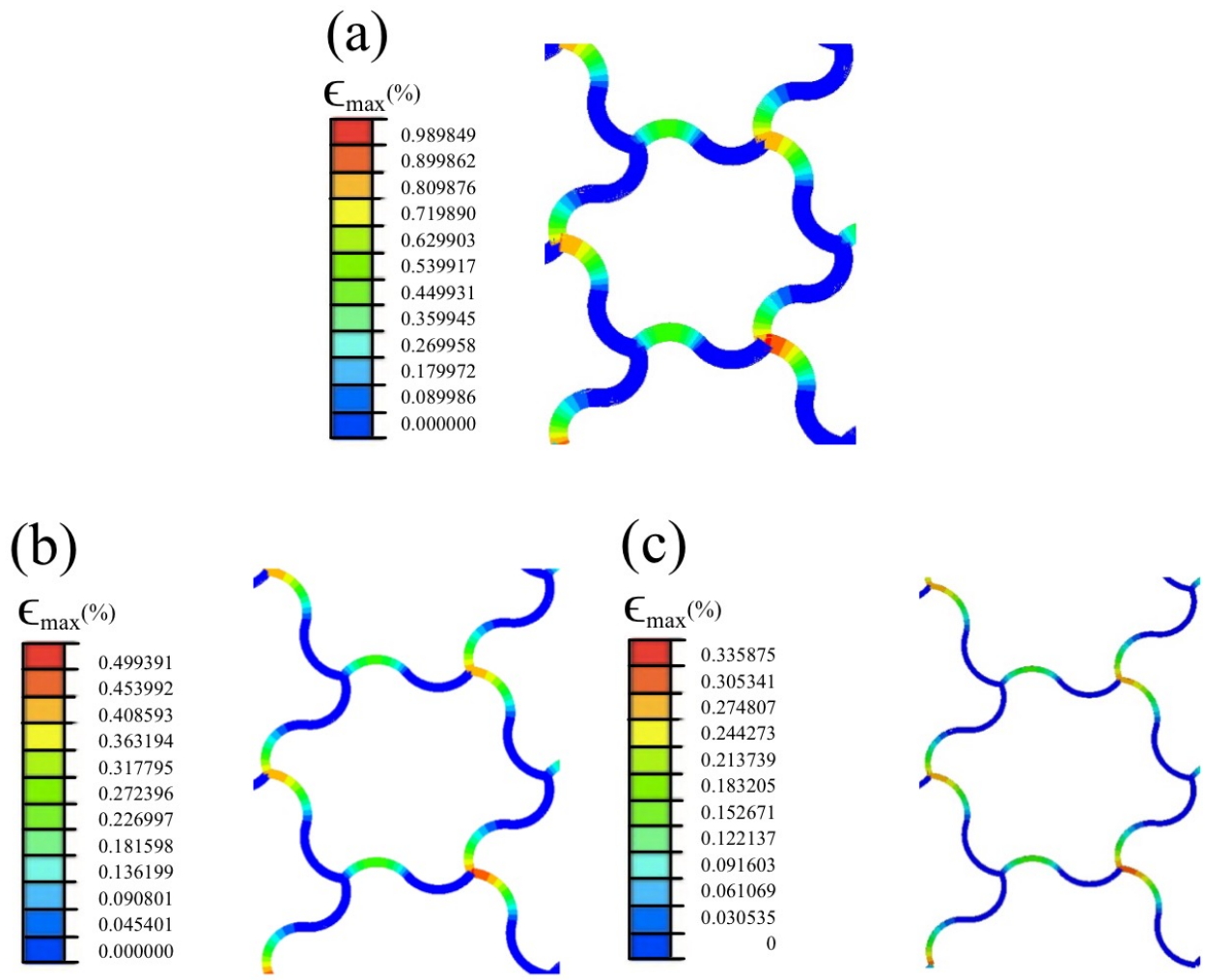


Figure 20: Maximum Strain of the nanomeshes from Finite Element Analysis for the traces of arc-angle 112.5 °and thickness of (a) 18nm, (b) 9nm and (c) 6nnm. Given that the deformation is periodic, only representative nanomeshes are shown.

quite closely with the FEA results. Thus, it can be asserted that the analytical model and the FEA results are in good agreement.

In Figure 25, plots for three distinct $\frac{R}{t}$ ratios and the arc-angles 22.5°to 153°represent the normalized stretchability of the structures, which is the ratio of applied strain to intrinsic fracture strain of the traces.

### 4.5 Results and Discussion

Here, from the figure 16, it can be seen that for arc-angle 22.5°to 153°the intrinsic effective modulus of the hexagonal nanomesh structure ranges from 0.00120586 GPa to 0.358748 GPa for $\frac{R}{t}$=10, from 0.000150732 GPa to 0.0448435 GPa for $\frac{R}{t}$=20 and from 0.000544661 GPa to 0.013287 GPa for $\frac{R}{t}$=30 along the x-direction, where arc-shaped traces' radius, R=180nm, width t=18,9,6nm and out of plan thickness, h=5nm, So, in our analysis the hexagonal

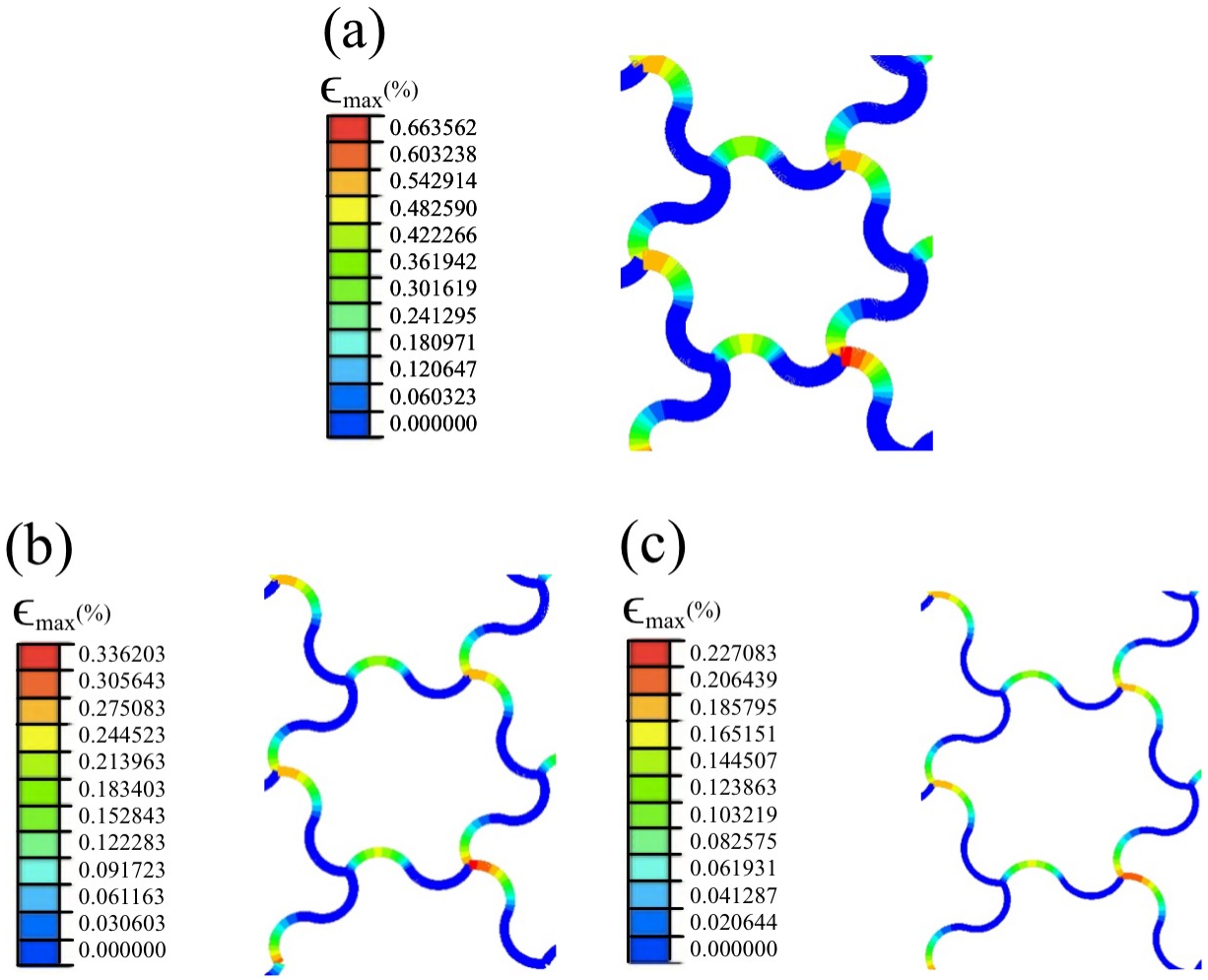


Figure 21: Maximum Strain of the nanomeshes from Finite Element Analysis for the traces of arc-angle 135 °and thickness of (a) 18nm, (b) 9nm and (c) 6nnm. Given that the deformation is periodic, only representative nanomeshes are shown.

nanomesh structures of arc-angle 153 °, radius 180 nm, width 6nm and thickness 5nm showed the lowest elastic modulus. These elastic modulus are gained by a bilayer structure of gold of young's modulus $E_{gold} = 79$ GPa [24] and width of 6 to 18 nm.

Similarly, for stretching the structures along the y-direction, the structure of arc-angle 153°, radius 180 nm, width 6nm and thickness 5nm showed the lowest elastic modulus (Figure 18).

The resistance of the material to elastic or stretchy deformation can be measured by the elastic modulus and the low elastic modulus means the structure is like floppy and can get stretched hugely under tension [2]. So, the hexagonal nanomesh structures are hugely stretchable under tensile force and it can show almost 158000 times more stretch-ability compared to a thin gold film depending on the geometric parameter. The effective moduli in x and y direction for the hexagonal nanomeshes are very close [41] which makes the hexagonal nanomesh structures to have almost same properties along both x- and y-directions. So, it can be predicted that the properties in the other directions will also be similar and that

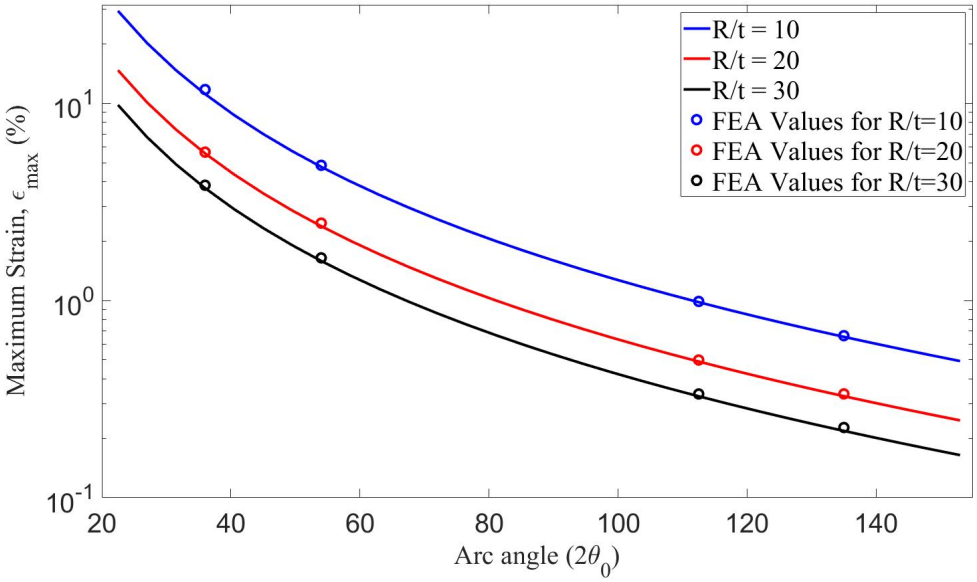


Figure 22: Maximum Strain of the nanomeshes versus arc angle ($2\theta_0$)

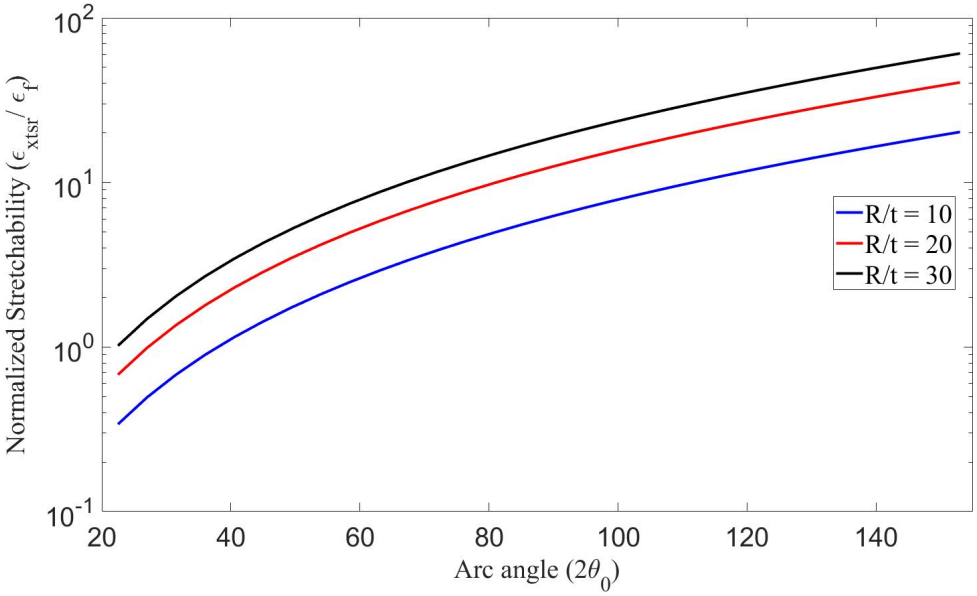


Figure 23: Normalized Stretchability of the nanomeshes versus arc angle ($2\theta_0$)

will make the hexagonal structure almost isotropic in mechanical behavior, which is very desirable in stretchable electronics, bio-sensors, skin-like elastomers and bio-electronics [11] [1].

The maximum strain of the nanomeshes due to stretching along the x-direction for the traces of radius 180nm and arc-angle 22.5 °to 153 °ranges from 0.493415% to 29.4517% for 10nm thickness, 0.246708 % to 14.7259% for 20nm thickness and 0.164472 % to 9.81724% for 6nm thickness ( Figure 22).

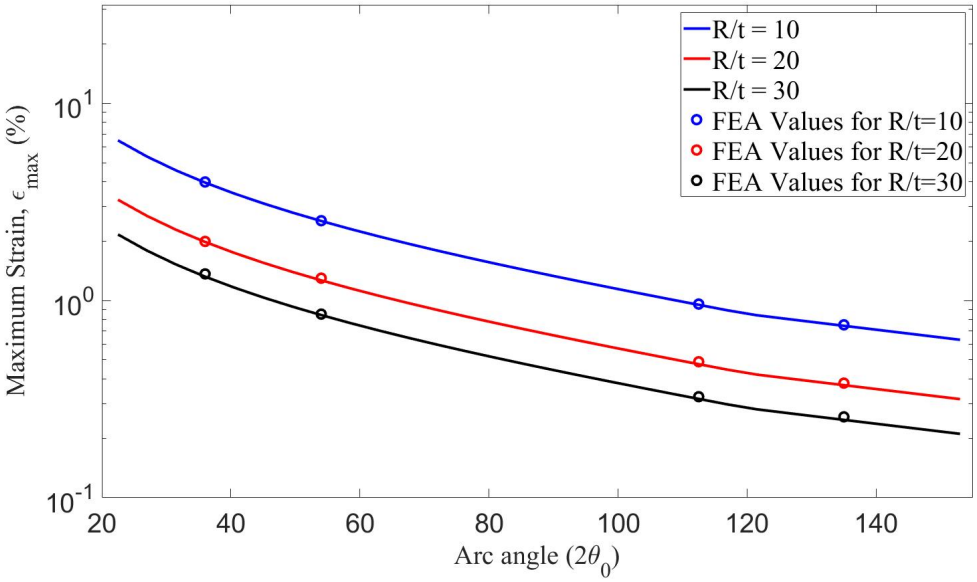


Figure 24: Maximum Strain of the nanomeshes versus arc angle ($2\theta_0$)

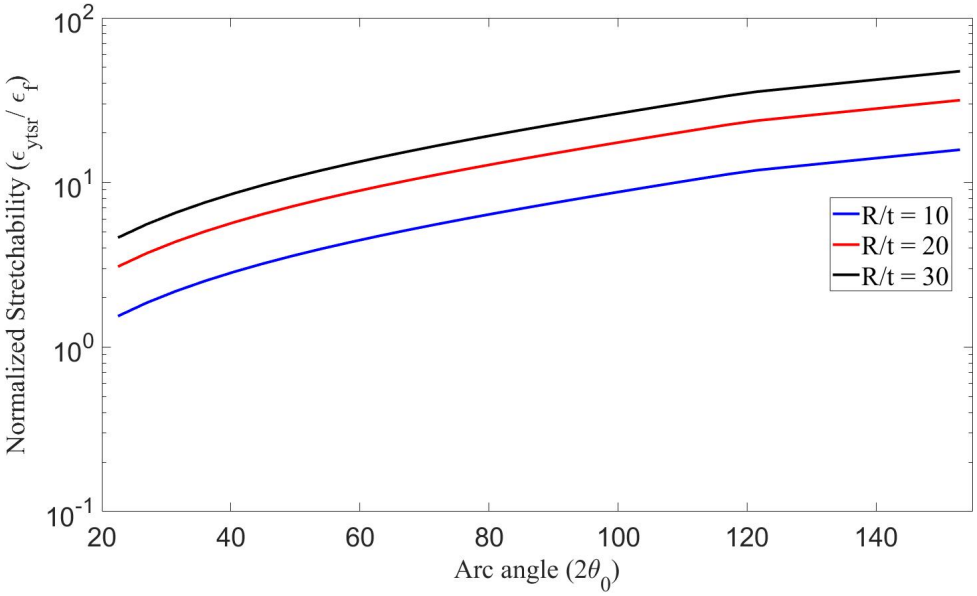


Figure 25: Normalized Stretchability of the nanomeshes versus arc angle ($2\theta_0$)

The maximum strain of the nanomeshes due to stretching along the y-direction ranges from 0.6325669% to 6.4912611% for 10nm thickness, 0.3163% to 3.2456% for 20nm thickness and 0.210856 % to 2.16375% for 6nm thickness ( Figure 24).

The normalized stretchability of the nanomeshes for similar trace radius and arc-angles ranges from 0.339539 to 20.2669 for 10nm thickness, 0.679077 to 40.5338 for 20nm thickness and 1.01862 to 60.8007 for 6nm thickness along the x-direction( Figure 23).

Similarly, the normalized stretchability of the nanomeshes for same trace radius and arc-

angles ranges from 1.5405 to 15.8086 for 10nm thickness, 3.081065 to 31.61720419 for 20nm thickness and 4.6215 to 47.4258 for 6nm thickness along the y-direction ( Figure 25).

So, with increasing arc-angle and reduction of thickness maximize the stretchability to sixty times larger than the intrinsic fracture strain of the traces, $\epsilon_f = 5.9\%$ [24] which is about 350% along the x-direction and almost forty seven times which is 277% along the y-direction and make the structure ultra-stretchable which is very useful for biocompatible instruments.

# CHAPTER V

## Conclusion and Future Work

### 5.1 Conclusion

The mechanical characteristics of the hexagonal nanomesh structures are investigated by theoretical models that are supported by FEA data. The hexagonal nanomesh structures for same radius and thickness show lower elastic moduli with the increasing arc-angle of the serpentine traces. Low elastic modulus which means these have very less stiffness and rigidity. In accordance with the lower stiffness, they show higher stretchability with the increasing arc-angle which makes it very suitable for bio-integrated applications. So, the serpentines with smaller thickness and higher arc-angle exhibits lower strain or higher stretchability. The analytical expressions will help to characterize the square and triangular serpentine nanaomesh structures also changing the direction of axial and transverse shear forces and in overall design of nanomesh structures consists of arc-shaped horizontal and inclined traces.

### 5.2 Future Work

Many aspects of stretchable electronics and serpentine structure need further investigation, such as exploring different materials, shapes, direction of applied forces, density and overall performances. The goal of future effort will be to solve increasingly complicated patterns of nanomeshes. Though the mechanical properties of the hexagonal nanomesh structures are expected to be similar in both x and y direction [41], the next immidiate step of this work will be to verify the analytical predictions of all the mechanical properties along the y-direction with FEA results using the described procedure in this work.

The same analysis will be done for sinusoidal shaped serpentine traces on hexagonal nanomeshes and for triangular and square nanomesh structures, as the square nanomeshes of straight traces have higher stretchability and lower stiffness compared to hexagonal and triangular structures [41]. The overall performances of these three structures will be compared based on the transparency and similar geometric parameters.

Using other materials on this structure like silver/silver chloride (Ag/AgCl), platinum (Pt), Iridium oxide (IrOx), and platinum-iridium oxide (Pt/IrOx) to be used on micro-electrodes[20], graphene, boron nitride, and transition metal dichalcogenides for flexible and stretchable eletronics to investigate and compare their performances.

## REFERENCES


[1] *Design and optimization of isotropic stretchable strain sensors for multidirectional monitoring - iopscience*, https://iopscience.iop.org/article/10.1088/1361-665X/ac319e/meta, (Accessed on 07/10/2022).

[2] *Elastic moduli - an overview — sciencedirect topics*, https://www.sciencedirect.com/topics/materials-science/elastic-moduli#:~:text=Elastic%20modulus%20measures%20the%20resistance,down%20very%20little%20when%20pushed)., (Accessed on 07/10/2022).

[3] *File:graphen.jpg - wikipedia*, https://en.wikipedia.org/wiki/File:Graphen.jpg#filehistory, (Accessed on 07/22/2022).

[4] *Linear vs quadratic fe elements - fea tips*, https://featips.com/2019/03/29/linear-vs-quadratic-fe-elements/, (Accessed on 07/08/2022).

[5] *Stiffness vs. strength: Differences and key factors to note — rapiddirect*, https://www.rapiddirect.com/blog/stiffness-of-material/#What_is_Stiffness_of_Material, (Accessed on 07/13/2022).

[6] Naveed Anwar and Fawad Ahmed Najam, *Structural cross sections: analysis and design*, Butterworth-Heinemann, 2016.

[7] Donald R Askeland, Pradeep Prabhakar Phulé, Wendelin J Wright, and DK Bhattacharya, *The science and engineering of materials*, (2003).

[8] E Baumgart, *Stiffness—an unknown world of mechanical science*, Injury **31** (2000), no. Suppl 2, B14–23.

[9] FP Beer, ER Johnston, JT DeWolf, and DF Mazurek, *Mechanics of materials. 7th_edition*, New York. MeGraw-Hill Education Ltd (2015).

[10] Arthur Peter Boresi, Richard Joseph Schmidt, Omar M Sidebottom, et al., *Advanced mechanics of materials*, vol. 6, Wiley New York, 1985.

[11] Shuo Chen, Lijie Sun, Xiaojun Zhou, Yifan Guo, Jianchun Song, Sihao Qian, Zenghe Liu, Qingbao Guan, Eric Meade Jeffries, Wenguang Liu, et al., *Mechanically and biologically skin-like elastomers for bio-integrated electronics*, Nature communications **11** (2020), no. 1, 1–8.

[12] Wentao Dong, Chen Zhu, Dong Ye, and YongAn Huang, *Optimal design of self-similar serpentine interconnects embedded in stretchable electronics*, Applied Physics A **123** (2017), no. 6, 428 (en).

[13] Zhichao Fan, Yihui Zhang, Qiang Ma, Fan Zhang, Haoran Fu, Keh-Chih Hwang, and Yonggang Huang, *A finite deformation model of planar serpentine interconnects for stretchable electronics*, International Journal of Solids and Structures **91** (2016), 46–54 (en).

[14] Chuan Fei Guo, Tianyi Sun, Qihan Liu, Zhigang Suo, and Zhifeng Ren, *Highly stretchable and transparent nanomesh electrodes made by grain boundary lithography*, Nature communications **5** (2014), no. 1, 1–8.

[15] Ho Young Jang, Seoung-Ki Lee, Sang Hyun Cho, Jong-Hyun Ahn, and Sungho Park, *Fabrication of metallic nanomesh: Pt nano-mesh as a proof of concept for stretchable and transparent electrodes*, Chemistry of Materials **25** (2013), no. 17, 3535–3538.

[16] Amar Khennane, *Introduction to finite element analysis using matlab® and abaqus*, CRC Press, 2013.

[17] Sang Jin Kim, Kyoungjun Choi, Bora Lee, Yuna Kim, and Byung Hee Hong, *Materials for flexible, stretchable electronics: graphene and 2d materials*, Annual Review of Materials Research **45** (2015), 63–84.

[18] Stephanie P Lacour, Sigurd Wagner, Roger J Narayan, Teng Li, and Zhigang Suo, *Stiff subcircuit islands of diamondlike carbon for stretchable electronics*, Journal of applied physics **100** (2006), no. 1, 014913.

[19] Sung Min Lee, Seungwoo Oh, and Suk Tai Chang, *Highly transparent, flexible conductors and heaters based on metal nanomesh structures manufactured using an all-water-based solution process*, ACS applied materials & interfaces **11** (2019), no. 4, 4541–4550.

[20] Chunyan Li, Raj K Narayan, Pei-Ming Wu, Neena Rajan, Zhizhen Wu, Neal Mehan, Eugene V Golanov, Chong H Ahn, and Jed A Hartings, *Evaluation of microelectrode materials for direct-current electrocorticography*, Journal of neural engineering **13** (2015), no. 1, 016008.

[21] Teng Li, Zhigang Suo, Stéphanie P Lacour, and Sigurd Wagner, *Compliant thin film patterns of stiff materials as platforms for stretchable electronics*, Journal of materials research **20** (2005), no. 12, 3274–3277.

[22] Yuhang Li, Bo Fang, Jiazhong Zhang, and Jizhou Song, *Surface effects on the wrinkling of piezoelectric films on compliant substrates*, Journal of Applied Physics **110** (2011), no. 11, 114303.

[23] Daryl L Logan, *A first course in the finite element method*, Cengage Learning, 2016.

[24] Yang Lu, Jun Song, Jian Yu Huang, and Jun Lou, *Fracture of sub-20nm ultrathin gold nanowires*, Advanced Functional Materials **21** (2011), no. 20, 3982–3989.

[25] Cheng Lv, Hongyu Yu, and Hanqing Jiang, *Archimedean spiral design for extremely stretchable interconnects*, Extreme Mechanics Letters **1** (2014), 29–34 (en).

[26] Louis Melville Milne-Thomson, *Theoretical aerodynamics*, Courier Corporation, 1973.

[27] Akihito Miyamoto, Sungwon Lee, Nawalage Florence Cooray, Sunghoon Lee, Mami Mori, Naoji Matsuhisa, Hanbit Jin, Leona Yoda, Tomoyuki Yokota, Akira Itoh, et al., *Inflammation-free, gas-permeable, lightweight, stretchable on-skin electronics with nanomeshes*, Nature nanotechnology **12** (2017), no. 9, 907–913.

[28] Taisong Pan, Matt Pharr, Yinji Ma, Rui Ning, Zheng Yan, Renxiao Xu, Xue Feng, Yonggang Huang, and John A. Rogers, *Experimental and Theoretical Studies of Serpentine Interconnects on Ultrathin Elastomers for Stretchable Electronics*, Advanced Functional Materials **27** (2017), no. 37, 1702589 (en).

[29] Yi Qiang, Kyung Jin Seo, Xuanyi Zhao, Pietro Artoni, Negar H Golshan, Stanislav Culaclii, Po-Min Wang, Wentai Liu, Katherine S Ziemer, Michela Fagiolini, et al., *Bilayer nanomesh structures for transparent recording and stimulating microelectrodes*, Advanced Functional Materials **27** (2017), no. 48, 1704117.

[30] DWA Rees, *Strain energy*, Basic Solid Mechanics, Springer, 1997, pp. 225–268.

[31] John A Rogers, Takao Someya, and Yonggang Huang, *Materials and mechanics for stretchable electronics*, science **327** (2010), no. 5973, 1603–1607.

[32] Tsuyoshi Sekitani, Hiroyoshi Nakajima, Hiroki Maeda, Takanori Fukushima, Takuzo Aida, Kenji Hata, and Takao Someya, *Stretchable active-matrix organic light-emitting diode display using printable elastic conductors*, Nature materials **8** (2009), no. 6, 494–499.

[33] Tsuyoshi Sekitani, Yoshiaki Noguchi, Kenji Hata, Takanori Fukushima, Takuzo Aida, and Takao Someya, *A rubberlike stretchable active matrix using elastic conductors*, Science **321** (2008), no. 5895, 1468–1472.

[34] Kyung Jin Seo, Xun Han, Yi Qiang, Xuanyi Zhao, Yiding Zhong, Zhan Shi, and Hui Fang, *Wafer-scale, stretchable nanomeshes from an ultrathin-support-layer assisted transfer*, Applied Physics Letters **112** (2018), no. 26, 263101.

[35] Kyung Jin Seo, Yi Qiang, Ismail Bilgin, Swastik Kar, Claudio Vinegoni, Ralph Weissleder, and Hui Fang, *Transparent electrophysiology microelectrodes and interconnects from metal nanomesh*, ACS nano **11** (2017), no. 4, 4365–4372.

[36] Mohammad Shahabuddin, Thomas McDowell, Carl E Bonner, and Natalia Noginova, *Enhancement of electrochromic polymer switching in plasmonic nanostructured environment*, ACS Applied Nano Materials **2** (2019), no. 3, 1713–1719.

[37] Michael Smith, *Abaqus/standard user's manual, version 6.9*, Dassault Systèmes Simulia Corp, United States, 2009 (English).

[38] J. Song, *Mechanics of stretchable electronics*, Current Opinion in Solid State and Materials Science **19** (2015), no. 3, 160–170 (en).

[39] Yewang Su, Zhuangjian Liu, Shuodao Wang, Roozbeh Ghaffari, Dae-Hyeong Kim, Keh-Chih Hwang, John A Rogers, and Yonggang Huang, *Mechanics of stretchable electronics on balloon catheter under extreme deformation*, International Journal of Solids and Structures **51** (2014), no. 7-8, 1555–1561.

[40] Mohaddeseh Vafaiee, Manouchehr Vossoughi, Raheleh Mohammadpour, and Pezhman Sasanpour, *Gold-plated electrode with high scratch strength for electrophysiological recordings*, Scientific Reports **9** (2019), no. 1, 1–11.

[41] Sandra Vinnikova, Hui Fang, and Shuodao Wang, *Mechanics of regular-shape nanomeshes for transparent and stretchable devices*, Journal of Applied Mechanics **87** (2020), no. 10.

[42] Yan Wang, Sunghoon Lee, Tomoyuki Yokota, Haoyang Wang, Zhi Jiang, Jiabin Wang, Mari Koizumi, and Takao Someya, *A durable nanomesh on-skin strain gauge for natural skin motion monitoring with minimum mechanical constraints*, Science advances **6** (2020), no. 33, eabb7043.

[43] Sheng Xu, Yihui Zhang, Jiung Cho, Juhwan Lee, Xian Huang, Lin Jia, Jonathan A Fan, Yewang Su, Jessica Su, Huigang Zhang, et al., *Stretchable batteries with self-similar serpentine interconnects and integrated wireless recharging systems*, Nature communications **4** (2013), no. 1, 1–8.

[44] Shixuan Yang, Becky Su, Ghassan Bitar, and Nanshu Lu, *Stretchability of indium tin oxide (ITO) serpentine thin films supported by Kapton substrates*, International Journal of Fracture **190** (2014), no. 1-2, 99–110 (en).

[45] Yihui Zhang, Shuodao Wang, Xuetong Li, Jonathan A. Fan, Sheng Xu, Young Min Song, Ki-Joong Choi, Woon-Hong Yeo, Woosik Lee, Sharaf Nafees Nazaar, Bingwei Lu, Lan Yin, Keh-Chih Hwang, John A. Rogers, and Yonggang Huang, *Experimental and Theoretical Studies of Serpentine Microstructures Bonded To Prestrained Elastomers for Stretchable Electronics*, Advanced Functional Materials **24** (2014), no. 14, 2028–2037 (en).

[46] Qian Zhao, Ziwei Liang, Bingwei Lu, Ying Chen, Yinji Ma, and Xue Feng, *Toothed Substrate Design to Improve Stretchability of Serpentine Interconnect for Stretchable Electronics*, Advanced Materials Technologies **3** (2018), no. 11, 1800169 (en).

[47] Yadong Zhou and Qingguo Fei, *Evaluating deformation modes of sandwich serpentine structures for high stretchability*, Thin-Walled Structures **157** (2020), 107087 (en).

VITA

OISHWARYA BHOWMIK

Candidate for the Degree of

Master of Science

Thesis: DESIGN OF
ULTRA-STRETCHABLE NANOMESH
STRUCTURES

Major Field: Mechanical and Aerospace Engineering

Biographical:

Education:

Completed the requirements for the Master of Science in Mechanical and Aerospace Engineering at Oklahoma State University, Stillwater, Oklahoma in July, 2022.
Completed the requirements for the Bachelor of Science in Mechanical Engineering at Bangladesh University of Engineering and Technology, Dhaka, Bangladesh in 2018.

Experience:

Graduate Research Assistant, Mechanics and Materials Laboratory, Oklahoma State University (January 2020- July 2022). Graduate Teaching Assistant, Oklahoma State University (August 2021-December 2021).